TREATING MELANOMA IN AN EXPERIMENTAL SYSTEM BY TARGETING GLUTAMATERGIC SIGNALING AND PD-1 INHIBITION

by

ANN K. ROBINSON

A thesis submitted to the

School of Graduate Studies

Rutgers, The State University of New Jersey

In partial fulfillment of the requirements

For the degree of

Master of Science

Graduate Program in Microbiology and Molecular Genetics

Written under the direction of

Suzie Chen

And approved by

_____

_____

_____

New Brunswick, New Jersey

October, 2017

ABSTRACT OF THE THESIS

Treating melanoma in an experimental system by targeting glutamatergic signaling and PD-1 inhibition

By ANN K. ROBINSON

Thesis Director:

Suzie Chen

Melanoma is the most dangerous type of skin cancer due to the frequency of metastasis and resistance to therapies, including radiation, traditional chemotherapies, and targeted therapies. Drug resistance and immune evasion are two issues currently gaining attention in the areas of melanoma research and treatment. To combat drug resistance, various combination treatment strategies are under investigation. Immune checkpoint blockade, a popular area of immunotherapy, aims to harness a patient's cytotoxic T cell response to combat tumor growth. Previously, our group identified the ectopic expression of a normal neuronal receptor, metabotropic glutamate receptor 1 (mGluR1) in the etiology of melanoma development and pathogenesis. When aberrantly expressed in melanocytes, mGluR1 activates two of the most commonly dysregulated signaling cascades, MAPK and P13K/AKT pathways that promote cellular proliferation while inhibiting apoptosis. To interrupt signaling through mGluR1, we took advantage of the anti-glutamatergic activity of riluzole. Riluzole is an FDA approved drug for the treatment of amyotrophic lateral sclerosis (ALS). In the current study, in addition to

using riluzole as an antagonist to mGluR1, we also used a newly developed prodrug for riluzole, FC4157.

Tumor biopsies from patients who participated in our Phase 0 and 2 clinical trials with riluzole suggest those who benefit from the drug have suppression of angiogenesis and increased leukocyte numbers at the tumor-stroma interface. Based on these observations, we began to test in a preclinical experimental model system, the efficacy of combining either riluzole or FC4157 with PD-1 checkpoint blockade.

We observed a significant reduction in tumor volumes in animals receiving either riluzole or FC4157 in combination with PD-1 blockade, as compared to vehicle or monotherapy treated groups. Western blot analysis on excised tumor lysates showed evidence of alterations to PD-1 ligand and DNA damage markers, suggesting tumors from animals receiving combination therapies may be less likely to evade cytotoxic T cell responses and may respond better to anti-PD-1 treatment. Finally, ELISA array data from tumor tissues, splenic tissues, and serum samples indicate a dynamic, but ultimately favorable tumor microenvironment for an anti-tumor immune response.

ACKNOWLEDGEMENT

I would first like to express my appreciation and gratitude to Dr. Suzie Chen for teaching me how to be a researcher and allowing me to work in her lab. I sincerely appreciate all your contributed time and effort.

I also would like to thank Dr. Audrey Minden and Dr. Sam Gunderson for agreeing to be part of my thesis committee.

This thesis would not be possible without collaboration from past and current members of the Chen lab. Thank you all for your contributions to this work and my development as a scientist.

Finally, I would like to express my gratitude to my family and network of friends who have been an incredible support system, both before and during my graduate school career.

PREVIOUS PUBLICATION ACKNOWLEDGMENT

Please allow this to serve as acknowledgment of the previous publication “New Approaches to Melanoma Treatment: Checkpoint Inhibition with Novel Targeted Therapy”, by Ann Robinson, published in Clinical Research in Dermatology, volume 4, edition 2. The current work, also written by Ann K. Robinson, contains small sections of shared text with this previous publication.

TABLE OF CONTENTS

ABSTRACT OF THE THESIS……ii

ACKNOWLEDGEMENT……iv

PREVIOUS PUBLICATION ACKNOWLEDGMENT……v

TABLE OF CONTENTS……vi

LIST OF FIGURES……ix

INTRODUCTION……1

PART I: MELANOMA……1

A. Melanoma……1

B. Earlier Melanoma Treatments……2

C. Recent Melanoma Treatments……3

D. Immunotherapy for Melanoma Treatment……4

PART II: METABOTROPIC GLUTAMATE RECEPTOR 1 (GRM1)……7

A. Metabotropic glutamate receptor 1 (Grm1) ……7

B. GRM1 Signaling……8

C. Riluzole……9

D. FC4157 – Riluzole Prodrug……10

PART III: T CELL DEVELOPMENT & ACTIVITY……12

A. T Cell Development……12

B. Immune Checkpoints: PD-1, PD-L1……13

METHODS……20

A. Cell Culture & Transfection……20

B. Animal Models……..21

C. Cell Preparation & Injection……..21

D. Treatment Groups……22

E. Tumor Measurements……..23

F. Blood Collection……23

G. Tissue Collection……..24

H. ELISA Immunoassay……24

I. Tumor Protein Lysates……..24

J. Cellular Protein Lysates……25

K. Western Blots……26

L. Protein Lysate Preparation……27

M. Antibodies……27

RESULTS……29

PART I: INJECTION AND TREATMENT PROTOCOL OPTIMIZATION……29

PART II: TUMOR VOLUME MEASUREMENTS & SURVIVAL……32

PART III: WESTERN BLOTS USING TUMOR TISSUE PROTEIN LYSATES……33

A. Reduced PD-L1 expression in tumors from combination treatment groups..33

B. Increased γH2AX expression in tumors from combination therapy groups….33

PART IV: CYTOKINE EXPRESSION IN TUMORS, SPLEENS, AND SERUM……35

A. ELISA array shows differences in cytokine expression between tumor sets…36

B. ELISA array shows increased cytokine expression in spleens from all treatment groups, notably, the combination one group……37

C. ELISA array shows increased cytokine expression in serum from αPD-1, rat IgG treatment groups……38

PART V: CHEMOKINE EXPRESSION IN TUMORS, SPLEENS, AND SERUM……41

A. ELISA array shows increased chemokine expression in tumors, spleens from monotherapy treatment groups……42

B. ELISA array shows increased chemokine expression in serum from all treatment groups……43

DISCUSSION……45

FUTURE DIRECTIONS……53

REFERENCES……55

FIGURES……60

LIST OF FIGURES

Figure 1. Signaling through mGluR1 promotes proliferation and generates anti-apoptotic signals……..61

Figure 2. Optimal T cell activation requires antigen presentation and co-stimulatory signals……..62

Figure 3. PD-1 engagement by ligand PD-L1 allows T cells to distinguish between normal cells and harmful or foreign cells. ……63

Figure 4. Treatment schedule and drug concentrations administered to each treatment group. ……64

Figure 5. . Tumor volumes in C57BL/6 animals, injected with $2.5x10^5$ Mass20 cells, after four weeks of treatment……65

Figure 6. Average tumor volumes, by group, normalized to tumor volume at time point 1. ……66

Figure 7. Survival by treatment group, based on tumor volumes……67

Figure 8. Reduced PD-L1 expression in protein lysates from tumor tissue from combination one and two treatment groups. ……68

Figure 9. Increased γH2AX expression in protein lysates from tumors developed on animals treated with riluzole and FC4157, as either a monotherapy or part of a combination therapy with PD-1 blockade. ……69

Figure 10. Cytokine expression patterns vary between tumor sets one and two……70

Figure 11. Cytokine expression based on averages of each treatment group from tumor sets one and two. ……71

Figure 12. Cytokine expression levels in splenic tissue. ……72

Figure 13. Changes to cytokine expression in serum, as compared to time point zero….73

Figure 14. Percent change in cytokine expression between time point 0 and endpoint in serum samples. ……74

Figure 15. Changes to chemokine expression, as compared to vehicle treatment……..75

Figure 16. Chemokine expression based on averages of each treatment group from tumor sets one and two. ……76

Figure 17. Chemokine expression based on ELISA array analysis of splenic tissue……..77

Figure 18. Percent change in average chemokine expression between time point 0 and endpoint in serum samples. ……78

INTRODUCTION

Part I: Melanoma

A. Melanoma

Melanoma arises when melanocytes, the pigment producing cells of the epidermis, become transformed by mutations which can allow abnormal proliferation and unrestricted cell growth. The lesions resulting from radial growth of melanocytes are typically brown or black, as melanocytes produce the pigment melanin, but can also be pink, tan, or white. In addition to color, melanocytic lesions are usually asymmetrical, larger than 6mm in diameter, and have an unsymmetrical or jagged border(1, 2). If a freckle or mole begins evolving over time and shows any of these traits, health professionals advise visiting a dermatologist to determine whether treatment is necessary(1). When melanoma is diagnosed in the early radial growth stage, the most common treatment is surgical resection of the malignant tissue. If melanoma goes undiagnosed or recurs after initial resection, radial cell growth can advance to vertical growth, allowing malignant cells to invade the basement membrane. This marks a transition to advanced melanoma which has high potential to metastasize to sensitive areas, most commonly the lungs and brain(2). In addition to the high incidence of recurrence and risk of metastasis associated with melanoma, in many cases, advanced melanoma is refractory to most available therapies, making the disease difficult to treat, contributing to melanoma's reputation as the most dangerous type of skin cancer(1, 3).

While melanoma is less common than basal or squamous cell carcinomas, the number of melanoma cases in the United States continues to increase. This year, the

American Cancer Society expects over 85,000 new cases of melanoma to be diagnosed and about 10,000 people to die from the disease(1).

B. Earlier Melanoma Treatments

Surgical resection is the choice of treatment for early stage melanoma. However it is not uncommon for melanoma tumors in advanced stages to become large or numerous, as well as invasive to surrounding normal tissue. For these reasons, surgical resection is not typically a viable treatment option for later stage melanoma patients. In lieu of surgery, these patients undergo various forms of chemotherapeutic and/or radiation therapies(3). Whole brain radiation therapy (WBRT) is commonly used in patients with brain metastases, however, patient survival rates did not drastically improve, as compared to patients who received only palliative care. Additionally, WBRT has been shown to negatively impact quality of life for some patients receiving this treatment as an adjuvant to other therapies (4, 5). Because of these drawbacks, WBRT has been limited to use in patients with widespread or large volume brain metastases.

An alternative radiation approach to WBRT, is stereotactic radiosurgery (SRS), also known as CyberKnife or Gamma Knife treatment. This modality delivers high-dose radiation by using multiple radiation beams that converge at a defined point where the tumor is located. Utilizing radiation in this grid-like manner allows delivery to a specific region, while preventing high doses of radiation exposure to adjacent, noncancerous areas(3). Delivery systems permit treatment of multiple metastases, however, only recently have the data emerged supporting its use for brain metastases. Recent studies have shown comparable improvements to survival in groups with a single secondary

tumor versus groups with as many as ten secondary tumors, however, melanoma-specific responses to this therapy have yet to be investigated(3, 6).

C. Recent Melanoma Treatments

Malignant melanoma cells can quickly develop resistance to traditional therapies such as radiation. To combat this problem, the focus of melanoma treatment has shifted towards therapies targeting specific mutations identified as “drivers” of this disease. Many cases of melanoma can be attributed to aberrant activation of signaling cascades responsible for regulating cell growth, such as the mitogen-activated protein kinase (MAPK) pathway. Activating mutations in components of this signaling cascade promote deregulated cell proliferation and suppress apoptosis. Sorafenib, a multi-kinase inhibitor, has been used to target multiple steps in the MAPK pathway and is FDA approved for treating several cancer types(7). Vemurafenib and dabrafenib are both used to treat melanoma patients with a point mutation substituting glutamic acid for valine at amino acid reside 600 within the BRAF gene, the most common mutation associated with melanoma. Vemurafenib was the first oral targeted mutant BRAF inhibitor approved by the FDA to treat patients with unresectable or metastatic melanoma expressing mutated BRAF. Metastatic melanoma patients experienced increased overall survival when treated with vemurafenib versus dacarbazine, a cytotoxic chemotherapeutic agent, and 37% of patients saw regression of intracranial tumors(8, 9). Dabrafenib received FDA approval shortly after vemurafenib and achieved improved progression-free survival and anti-tumor activity for intracranial lesions in the 30-40% range(3).

Despite initial success with targeted therapies, many patients experience disease recurrence or cease responding to treatment. High recurrence and resistance rates suggest melanoma can circumvent signaling blockades resulting from targeted therapy by inducing novel mutations, which allow the disease to progress. For this reason, identifying alternative treatment targets for melanoma remains critical.

D. Immunotherapy for Melanoma Treatment

As targeted therapies continue to encounter biological roadblocks, a relatively new approach, immunotherapies, gain more attention. Immunotherapy seeks to activate or enhance a patient's immune response against tumor-specific antigens, allowing the host's immune system to target cancer cells specifically(10). One of the earliest immunotherapies used to treat melanoma was administration of high-dose interleukin-2 (HD IL-2), a cytokine promoting T-cell proliferation(11). About 16% of melanoma patients enrolled in a clinical trial showed durable responses to HD IL-2 treatment(12). Similar results were observed in a renal cell carcinoma clinical trial, which led to FDA approval of HD IL-2 treatment for both immunogenic diseases. Unfortunately, the promising results in clinical trials were eventually overshadowed by the high toxicity observed in many patients. Lower doses of IL-2 showed fewer adverse effects, but were inferior to HD IL-2 treatment in generating durable anti-tumor responses(13).

More recently, BioVex, a subsidiary of Amgen (Thousand Oaks, CA) developed talimogene laherparepvec (T-VEC), an attenuated derivative of herpes simplex virus type 1 with the capability to selectively replicate within tumor cells. In addition to targeting tumor cells specifically, the virus includes a gene encoding granulocyte macrophage

colony-stimulating factor (GM-CSF), which results in local production of the cytokine and allows for antigen-presenting cell recruitment to help promote durable immune responses(14). T-VEC was the first oncolytic virus to be approved by the United States to treat locally advanced or unresectable melanoma(15). In one clinical trial, patients with unresectable, stage III or IV melanoma were treated with T-VEC or GM-CSF. Patients in the T-VEC arm showed improved durable and overall response rates versus patients in the GM-CSF arm. Patients receiving the oncolytic virus also had more than a 20% reduced risk of death after completing the clinical trial. Additionally, this clinical trial showed T-VEC had a tolerable safety profile(14). Despite initial excitement, clinical trials have shown T-VEC to have limited clinical efficacy as a monotherapy and reduced efficacy when used as a secondary or tertiary alternative to other immunotherapy strategies(14, 15).

While oncolytic viruses like T-VEC rely on a successfully initiated viral lytic cycle to destroy tumor cells, other immunotherapies utilize the theory of intrinsic tumor immune surveillance to combat disease. Tumor immune surveillance is the process by which cells of both innate and adaptive immune responses regularly identify cancerous or pre-cancerous cells and destroy them before they can become problematic(16). Over the past few decades, evidence from animal and human cancer models has emerged supporting the idea that the immune system is crucial to controlling the ever-growing population of malignant cells. When these normally efficient surveillance mechanisms are overwhelmed or thwarted by a repertoire of tumor cell defense mechanisms, though, malignant cells proliferate and disease progresses(16). Immunotherapies seek

to counteract the immunosuppressive tactics employed by tumor cells to promote an anti-tumor immune response and combat disease.

Part II: Metabotropic Glutamate Receptor 1 (Grm1)

A. Metabotropic glutamate receptor 1 (Grm1)

Metabotropic glutamate receptor 1 (gene: GRM1, human; Grm1, mouse; protein: mGluR1) is a seven transmembrane G-protein coupled receptor normally expressed in the central nervous system where its natural ligand L-glutamate functions as a neurotransmitter(17). While functional glutamatergic signaling in melanocytes was previously observed, our lab was the first to focus on the role of metabotropic glutamate receptor 1, specifically, in melanoma development and progression(17, 18).

A transgenic mouse model, TG-3, developed pigmented lesions on the skin surface with progression to distant organs, including lymph nodes, brain, and lungs. Histological analysis confirmed the lesions as melanoma, while molecular gene mapping identified several copies of the transgene, clone B, inserted into intron 3 of the gene encoding mGluR1. Subsequent protein and RNA assessment studies detected mGluR1 expression in tumor-bearing ears, but not in noncancerous ear tissue. We hypothesize that ectopic expression of a neuronal receptor, mGluR1, in melanocytes, where mGluR1 expression is not endogenous, results in tumor development. To test our hypothesis on the causative role of *Grm*1 in melanoma development, we generated another transgenic mouse line featuring *Grm*1 cDNA under the control of a melanocyte-specific promoter, dopachrome tautomerase. As this transgenic model developed melanoma lesions very similar to the TG-3 model, we concluded that ectopic *Grm1* expression alone, even in the absence of other known activating mutations in downstream pathways, is sufficient to induce spontaneous metastatic melanocytic neoplasia *in vivo(*19*)*. Further

investigation identified mGluR1 expression in over 80% of human melanoma cell lines and 60% of human melanoma biopsies(17).

To elucidate how mGluR1 expression affects downstream signaling pathways, our lab transfected exogenous mouse *Grm*1 cDNA into immortalized, nontumorigenic, mGluR1-negative mouse melanocytes isolated from C57BL/6, known as melanA. Several stable clones, called Mass clones, were isolated and, when injected subcutaneously, were very tumorigenic in both immune-competent syngeneic C57BL/6 and immune-compromised nude mice. We observed robust tumor formation, angiogenesis, and invasiveness to lung and muscle tissue. Functionality assays showed functional and sustained Grm1 expression, which was required to maintain the tumorigenic phenotype and establish autocrine loops, generating enhanced levels of extracellular glutamate, the natural ligand of mGluR1, for constitutive activation of the receptor(20, 21).

B. GRM1 Signaling

When mGluR1 binds its natural ligand, L-glutamate, the receptor couples to $G_{\alpha/q11}$ subunits, which hydrolyse phosphatidylinositol (4,5)-biphospthate (PIP2) to generate two second messengers, inositol triphosphate (IP_3) and diacyl glycerol (DAG)(22). IP_3 promotes the release of calcium from the endoplasmic reticulum and DAG stimulates protein kinase C (PKC) which activates the MAPK and PI3K/AKT signaling cascades to promote cellular proliferation and inhibit apoptosis(21) (Figure 1). After establishing the connection between mGluR1 and downstream deregulated signaling pathways, we investigated compounds capable of suppressing or inhibiting the consequences of the constitutively activated receptor. The receptor's localization in the

cell membrane and expression limited to transformed melanocytes make it an attractive therapeutic target(17).

C. Riluzole

Our lab, with clinician collaborators, investigated riluzole, an FDA-approved therapy for amyotrophic lateral sclerosis (ALS), as a potential inhibitor for glutamatergic signaling in preclinical studies(23). Riluzole functions by upregulating type II excitatory amino acid transporter (EAAT2), reducing levels of extracellular glutamate, therefore preventing local glutamate toxicity and alleviating symptoms resulting from neuronal damage(24, 25). Our group showed riluzole could successfully disrupt glutamatergic signaling in malignant melanoma cells by interfering with glutamate release to the extracellular environment of mGluR1 expressing melanoma cells, thus limiting the availability of the ligand to bind mGluR1 and maintain receptor activation(26). Consequences of a reduction in released glutamate include a decrease in intracellular glutathione levels, an increase in intracellular reactive oxygen species (ROS) and reduced cell growth, as has been shown for many transformed cells including melanoma(27, 28). This preclinical work has been translated to the clinic in the form of phase 0 and phase II trials for patients with advanced melanoma(29, 30). During the phase 0 trial riluzole administration to these patients for 14 days resulted in suppression of MAPK and PI3K/AKT signaling and tumor involution for 34% of patients, independent of BRAF/NRAS mutational status(29). Of the patients enrolled in the phase II trial, 37% of patients receiving riluzole as a monotherapy experienced disease stability. However, inhibition of mGluR1 signal transduction alone failed to change clinical outcomes in

patients with advanced melanoma, like many treatment regiments utilize single targeted therapies(30). Currently, we are exploring therapeutic options using riluzole in combination with other targeted therapies like vemurafenib and rapamycin, radiation therapy, and novel immunotherapies(31, 32). In an effort to reduce recurrence and eventual disease progression, an ongoing phase I trial is exploring the efficacy of combining riluzole with Sorafenib.

D. FC4157 – Riluzole Prodrug

When delivered orally, riluzole experiences first-pass metabolism by CYP1A2, an isoform of cytochrome p450. In the liver, riluzole undergoes N-hydroxylation, resulting in the formation of a transient intermediate, which is quickly altered via O-glucuronidation. The final, inactive drug product is readily eliminated from the body. Due to heterogeneous expression of this cytochrome p450 isoform within the population, drug exposure to riluzole is highly variable between patients. To circumvent the issues arising upon metabolism of riluzole, our group worked with partners at the Fox Chase Chemical Diversity Center to generate several prodrugs, designed to bypass CYP1A2 metabolism. The ideal prodrug would be stable after hepatic metabolism, then cleaved in the plasma or target tissue to release riluzole(33). Using prodrugs, rather than parent drug riluzole, would help improve bioavailability, potentially cut down on drug-drug interactions, and facilitate dosing across patient demographics, therefore making mGluR1 inhibition treatment accessible to a wider patient population.

From the group of prodrug candidates, we identified one, FC4157, which, when orally administered to preclinical melanoma animal models daily at 1.7mg/kg, reduced

tumor volumes comparably to riluzole, similarly administered at 7.5mg/kg (Raj Shah, Suzie Chen, unpublished). In preclinical PK/PD studies using FC4157 versus riluzole, exposure to the parent drug riluzole doubled when administered in the pro-drug, FC4157, form (J. Pelletier, Fox Chase Chemical Diversity Center, unpublished). In this dissertation, we wanted to investigate the efficacy of FC4157 used as a monotherapy, as well as in combination with checkpoint inhibition, to determine how its use compared to riluzole in our preclinical model.

Part III: T Cell Development & Activity

A. T Cell Development

T cell progenitors develop in the bone marrow before traveling to the thymus where the progenitors, thymocytes, develop into subsets of young T cells(34). In the thymus, genes encoding the T cell receptor (TCR), necessary for the recognition of foreign antigen and self-associated cells, undergo rearrangements, eventually generating a nascent TCR expressed on the cell surface. Once the receptor is expressed, the T cell interacts with major histocompatibility complex (MHC) proteins on the surface antigen presenting cells (APCs) like dendritic cells or thymic cortical epithelial cells. These interactions employ negative and positive selection to prevent the maturation of any immature T cell that either recognizes self MHC with high avidity or fails to recognize self MHC at all. High avidity to self MHC could allow for autoimmune responses against non-foreign tissues, while lack of recognition could prevent initiation of antigen-specific T cell immune response(34). Additionally, the class of MHC, either class I or II, drives T cell development into cytotoxic CD8+ or helper CD4+ effector subsets, respectively(34). Cytotoxic CD8+ T cells are capable of killing target cells expressing specifically recognized antigens, while helper CD4+ T cells mediate immune responses through the production of pro-inflammatory cytokines and assist with activation of T and B cells(35).Only when immature T cells have passed both selection tests do they receive signals allowing them to mature. Once mature, these antigen-naïve T cells rely on chemokines and cytokines to direct their movement to peripheral or secondary lymphoid tissues. In the secondary lymphoid tissues, mature, naïve T cells

wait to be activated by APCs carrying antigen from a site of infection or inflammation. Dendritic cells play a critical role in presenting antigen on their MHC surface proteins, which can interact with the TCR of the T cell(34). Optimal T-cell activation depends not only on T cell recognition of both the antigen and self MHC complex on the APC, but also on binding between co-stimulatory CD28 on T cells and B7 molecules on APCs(36) (Figure 2). The generation of a robust, durable, anti-tumor T cell response depends first on T cell activation into the effector state, and second, recognition of tumor-specific antigen, which are regulated by a delicate balance of co-stimulatory and co-inhibitory signals(35, 37). The therapeutic value of T cells stems from their ability to selectively recognize antigen, destroy antigen-expressing cells, and organize diverse long term and shorter term immune responses(35).

B. Immune Checkpoints: PD-1, PD-L1

Many antigens, including cyclin-dependent kinase 4, β-catenin, gp100, TRP2, and different forms of cancer-testis antigens have been implicated in melanoma development and progression(34). Cancer immune surveillance, a theory hypothesizing that the immune system and T cells particularly, can and frequently do recognize cancer-specific antigens, has gained popularity(16). To circumvent the anti-tumor activity of the immune system, cancers employ an array of tactics to avoid triggering an immune response or to hide from a response when it does occur(16, 34). One of the best understood immune-evasion techniques involves the exploitation of immune checkpoints(37). Immune checkpoints are inhibitory pathways responsible for maintaining self-tolerance and regulating the duration and amplitude of immune

responses. Immune checkpoints are widely found on many immune cell types, including T, B, and natural killer (NK) cells. Normally, these checkpoints protect normal, healthy tissue from cytotoxic immune responses, but manipulation of these pathways has been observed in many types of cancer, allowing tumor cells to escape the cytotoxic effector mechanisms of the immune system, especially T cells(35).

After being activated by recognition of MHC-antigen complex and co-stimulatory B7:CD28 engagement, T cells undergo a variety of cellular changes, including upregulation of the programmed cell death protein 1 (PD-1)(34, 38). PD-1 and its main ligand, programmed death ligand 1 (PD-L1 or B7-H1), is one of the most well studied immune checkpoints, particularly in cancer immunity(37). After activation, T cells become licensed to exit the secondary lymphoid tissues and can enter peripheral tissues. In the periphery, T cells encounter a drastically different environment from the secondary lymphoid tissues. As such, PD-1 becomes upregulated immediately upon activation, to ensure the variety of stimuli present in the peripheral tissues will not trigger an unnecessary and harmful immune response(34, 35).

Once in the peripheral tissues, successful T cell immunity depends heavily on distinguishing between foreign or infected cells and healthy ones. Normal, healthy cells avoid destruction by cytotoxic CD8+ T cells by presenting PD-L1 (Figure 3A). When a T cell's membrane bound PD-1 receptor is engaged by its ligand, PD-L1, downstream kinases within the T cell are prevented from engaging with the phosphatase SHP2, which inhibits further T cell activation and cytotoxic activity. It is likely that additional signaling pathways within the T cell are also impacted by PD-1 engagement, including

those pathways that govern the duration of contact permitted between T cells and APCs or target cells. Typically, this receptor-ligand interaction protects healthy cells from destruction during an immune response, but PD-L1 expression has been observed on many tumor types as well as myeloid-derived suppressor cells (MDSCs) within the tumor microenvironment. PD-L1 upregulation in the tumor microenvironment has been shown to inhibit anti-tumor local immune responses, allowing malignant tumor cells to evade immune responses and continue proliferating (Figure 3C). Melanoma was one of the first solid tumors where high PD-L1 expression was observed. PD-L1 expression and high levels of antigen exposure in the tumor microenvironment both promote T cell exhaustion or anergy, a state where overwhelmed T cells survive, but are incapable of carrying out cytotoxic activity or priming other immune cells to enhance the response(35, 38, 39).

PD-L1 expression in the cancer setting can be enhanced in two ways, either as a result of oncogenic signaling or as an adaptive response by the tumor to a pre-existing immune response. In glioblastomas, silencing phosphatase and tensin homolog (PTEN), a component in the regulation of P13K/AKT signaling cascade, allowed for the overexpression of PD-L1 on the tumor cell surface, suggesting the P13K/AKT pathway, also frequently mutated in melanoma, may play a causative role. Alternatively, PD-L1 expression can be induced by pro-inflammatory cytokines, like interferon-γ, or as a response to increased lymphocyte infiltration. Based on the tumor immune surveillance theory, it makes sense that malignant cells, after experiencing insult from a preliminary immune response, may upregulate PD-L1 to avoid further destruction(35).

Since identifying PD-L1 upregulation in many types of solid tumors, great attention has been paid to therapeutic agents capable of preventing or reversing the inhibitory effect of PD-L1 expression within the tumor microenvironment. As PD-1 and PD-L1 are membrane-bound, cell surface molecules, they can be easily targeted by small molecule inhibitors or antibodies to prevent receptor ligand engagement, therefore, reducing the downstream inhibitory effects on T cell activity. Additionally, the wide expression of PD-1 on various immune cell types may also alter the tumor microenvironment to better accommodate an anti-tumor response(35).

Once in the tumor microenvironment, T cells, particularly CD8+ T cells face an uphill battle. Tumor cells and immune suppressive cells supporting tumor growth produce metabolites and cytokines that inhibit T cell growth and maturation. Cells within the microenvironment compete for scarce nutrients, often starving out T and other immune cells, while rapidly proliferation tumor cells modify metabolic states to adapt. Metabolic and nutrient constraints can also negatively impact innate immune players, like dendritic cells, responsible for priming naïve T cells to ramp up the adaptive immune response. These factors, plus the overexpression of inhibitory PD-L1 on tumor cells or MDSCs eventually overwhelm T cells and interfere with effective anti-tumor responses(40).

If PD-1 engagement could be prevented, B and NK cells may also display higher anti-tumor activity, while proliferation of T regulatory cells, responsible for dampening immune responses, could be reduced. Early clinical trials with PD-1 specific antibodies

have also demonstrated the ability to reverse T cell anergy, making a specific anti-tumor response much more likely(35).

The first FDA approved antibody blockading immune checkpoints did not target PD-1, but a similar checkpoint molecule, cytotoxic T-lymphocyte antigen 4 (CTLA-4), which mainly regulates T cell maturation before activation occurs(35, 41). A few years later, two additional checkpoint inhibiting antibodies, pembrolizumab and nivolumab (Merck, Kenilworth, NJ; Bristol-Myers Squibb, New York, NY) both gained FDA approval within a few months of each other, for treating advanced or unresectable melanoma(41). Evidence supporting this relatively rapid approval came from a phase I clinical trial where nivolumab treatment led to regression of many types of solid tumors and promoted increased lymphocyte infiltration to distant metastases. A later clinical trial where nivolumab treatment was administered to patients with advanced melanoma over two years led to about 40% of patients showing an objective response, while either a mixed response or disease stabilization was observed in another 35% of patients(35). A clinical trial where pembrolizumab was administered to patients with advanced melanoma once every two weeks led to a 33% response rate. Upon following up with these patients 7.9 months after concluding treatment, clinicians observed ongoing responses in 89% of patients, suggesting not only an initial response to treatment, but more long term, durable responses were possible with pembrolizumab(42). More recently, the approvals of both drugs have been broadened to include other types of cancers including non-small cell lung cancer and renal cancer,

particularly for disease that has shown resistance to traditional or first-line therapies(41).

Since initial approval, preclinical and clinical data suggest that drugs blocking PD-1 may also have reduced risk for treatment-related adverse effects, as compared to CTLA-4 blocking ipilimumab(35). Recent research found PD-1 expression is not limited to cells of the hematopoietic lineage, such as lymphocytes, but can also be found on malignant melanoma cells. Results from early work suggest that PD-1 expression on tumor cells may provide a growth advantage, which can be counteracted by different blockade strategies, including PD-1 specific antibody treatment(10). Additionally, the broad expression of PD-1 on B and NK cells also leads some researchers to believe that PD-1 blockade may allow further anti-tumor immune activity from these cell types as well(35). Continued investigation may elucidate the utility of using PD-1 blockade to enhance immune responses as well as inhibit tumor cell growth beyond the scope of T cells alone.

Initial hope, spurred by promising clinical trials, has been dampened slightly, as some patients do not response as strongly to PD-1 blockade, while others continue to see disease progression, despite treatment(41). This concern, coupled with the knowledge that PD-L1 expression can be enhanced by inflammatory environments, like the tumor microenvironment, has led to the development of combination immunotherapy regimens(35, 41). Pre-clinical research has shown that combination PD-1 and CTLA-4 blockade results in rejection of pre-implanted B16 melanoma tumors more often than either modality alone. Further evidence of synergy between the two immune

checkpoint blockades also includes more favorable ratios of tumor infiltrating CD8+ T cells to regulatory T cells and increased interferon-γ production in combination therapy, as compared to monotherapy(38). Data from clinical trials also suggests that these two immune checkpoint blockades work synergistically when administered strategically(38, 41). Melanoma patients who receive ipilimumab and nivolumab as a combination regimen are typically those with aggressive, advanced disease or those who have ceased responding to targeted therapies like mutated BRAF inhibitors. Unfortunately, despite enhanced efficacy observed in some patients, combining these two checkpoint blockades has resulted in high toxicity as well as serious adverse effects for some patients, giving physicians pause. For this reason, investigation of PD-1 blockade in combination with other, more traditional, less toxic, and better tolerated therapies, is currently dominating preclinical and clinical research(41).

METHODS

A. Cell Culture & Transfection

Mass clone 20 (Mass20) and melanA were cultured in RPMI 1640 media (Sigma, St. Louis MO) supplemented with 10% fetal bovine serum (FBS) (Sigma, St. Louis MO) and 100 units/mL of penicillin/streptomycin (Sigma, St. Louis MO). All cells were incubated at 37°C with 10% CO_2. Mass20 cells were transfected with 3ug of plasmid DNA encoding red fluorescent protein (RFP) and 3ug of DNA encoding puromycin resistance. Transfection was carried out by mixing 26.3uL of sterile HEPES buffer (20mM HEPES with 150mM NaCl) and 11.2 uL DOTAP Liposomal Transfection Reagent (Roche, Basel SZ) and DNA. One day prior to transfection, $4x10^5$ Mass20 cells were plated in sterile 60mm culture plates. Thirty minutes before adding DNA and transfection reagents, RPMI 1640 media with 10% FBS was replaced with Opti-MEM Reduced Serum Media (Thermo Fisher Scientific, Carlsbad CA). The transfection mix was added and plates remained in the incubator for twenty-four hours. After twenty-four hours, transfected plates were washed with 1mL 1x sterile phosphate buffered saline (PBS), then exposed to 1mL 1x trypsin-EDTA (Thermo Fisher Scientific, Carlsbad CA). After centrifugation at 1000RPM for 10 minutes, cells were suspended in 3mL RPMI 1640 media with 10% FBS and penicillin/streptomycin. This volume was then split between three new 60mm culture plates and an additional 2mL of media was added to each plate. After incubating in the recently separated plates for twenty-four hours, 0.75ug/mL or 1ug/mL puromycin selection was added to each plate. Each plate of transfected Mass20 cells was maintained in these culture conditions until individual colonies could be isolated, about

4 weeks after initial transfection. To isolate colonies, 3.2mm sterile cloning disks (Sigma Aldrich, St. Louis MO) were soaked in 1x trypsin-EDTA, picked up using sterilized forceps, and gently placed onto individual colonies. After a few seconds, the cloning disk was picked up, using sterile forceps, and placed into one well of a 24-well sterile culture plate (Corning, Corning NY), containing 1.5mL of RPMI media with 10% FBS. When colonies in individual wells had grown to confluence, cells were exposed to .5mL of trypsin and transferred to 35mm plates (Corning, Corning NY), containing 1.5mL RPMI media with 10% FBS, without spinning. Individual colonies were screened for RFP expression using the Nikon Eclipse Ti fluorescence inverted microscope (Nikon, Tokyo JP) and confirmed by Western blot.

B. Animal Models

All mice were handled in accordance with the Chen lab animal protocol, as approved by the Institutional Animal Care and Use Committee at Rutgers University. For this study, we used fifty-four female, immunocompetent C57BL/6 animals from Taconic Biosciences (Hudson, NY). Hair was removed from the back and flanks of these animals by shaving, to facilitate injection, tumor detection, and tumor measurement. During the experiment, animals were maintained until individual tumor volumes reached 1500mm^3 or tumors became ulcerated.

C. Cell Preparation & Injection

Mass20 cells were cultured to confluence in 150mm culture plates. When confluent, plates were washed with 10mL 1x sterile PBS, then exposed to 10mL 1x trypsin-EDTA (Thermo Fisher Scientific, Carlsbad CA). After centrifugation at 1000RPM for 10 minutes,

cells were suspended in 1x sterile PBS to achieve $4.5x10^6$ cells/mL. To facilitate and reduce variability between injections, animals were temporarily put to sleep by exposure to Isoflurane (Piramal Healthcare, Mumbai IN) using the VetEquip (Pleasanton CA) isoflurane system and chamber. Matrigel matrix basement membrane (Corning, Corning NY) was added to the suspended cells to make a 1:1 ratio of Matrigel to PBS, distributing cells to $2.5x10^6$ cells/mL within the mixture. 100ul of the diluted Matrigel and cell mixture was injected, subcutaneously, to left or right flank of each animal.

D. Treatment Groups

When tumors became palpable, about 7-10 days post-injection, animals were designated into treatment groups, described as follows:

1. Vehicle One – DMSO: administered daily via oral gavage at a concentration comparable to riluzole
2. Vehicle Two – Rat IgG (BioXCell, West Lebanon NH): 100ug administered via intraperitoneal injection three times during the first week of treatment and once weekly thereafter
3. Riluzole (Selleckchem, Houston TX): 10mg/kg administered daily via oral gavage
4. **α**PD-1 (BioXCell, West Lebanon NH): 100ug administered via intraperitoneal injection three times during the first week of treatment and once weekly thereafter
5. FC4157 (Fox Chase Chemical Diversity Center, Doylestown PA): 1.7mg/kg administered daily via oral gavage

6. Riluzole + **α**PD-1: Administration and dosage as previously described for both modalities
7. FC4157 + **α**PD-1: Administration and dosage as previously described for both modalities

E. Tumor Measurements

Tumor width and length were measured twice weekly using a Vernier caliper. Tumor volumes were then calculated from both measurements using the following equation.

$$V=d^2 \times D/2$$

Where d is the smaller and D is the larger of the two measurements for each individual tumor. As many animals across the treatment groups featured multiple tumors, we averaged the volumes for each tumor to calculate a single tumor volume for each animal.

F. Blood Collection

Peripheral blood was collected from three representative animals from each treatment group at three time points during this experiment: before injecting Mass20 cells, before initiating treatment, and before sacrificing the animals. At each time point, 100-250uL of peripheral blood was drawn from the retro-orbital sinus using Fisherbrand capillary tubes (Hampton, NH). Peripheral blood was kept on ice at room temperature for at least 30 minutes after collection, then centrifuged at 10,000 RPM for 8 minutes to obtain serum. Serum was stored at -80˚.

G. Tissue Collection

When each tumor reached 1500mm^3, animals were sacrificed via cervical dislocation. All tumors were surgically removed post-mortem. Tumors from each animal were flash frozen in liquid nitrogen then stored at -80˚ or fixed in 10% formalin for 48 hours, then stored in 70% ethanol.

H. ELISA Immunoassay

Chemokine and cytokine ELISA arrays were performed in the lab of Dr. Andrew Zloza at the Rutgers Cancer Institute of New Jersey (New Brunswick, NJ). Tissues collected for use in the ELISA arrays include tumors and spleens from selected animals. After necropsy, the tissues were stored in chilled, 1x PBS and delivered promptly to CINJ.

I. Tumor Protein Lysates

Using a mortar and pestle, frozen tumors were mechanically pulverized. To maintain the sample temperature and prevent protein degradation, liquid nitrogen was added during the grinding process. Finely ground tumors were poured into chilled 10mL Falcon tubes. When the liquid nitrogen had evaporated off the ground samples, a volume of lysis buffer (below) appropriate to the size of the tumor was added to the chilled tubes. A laboratory homogenizer (OMNI International, Kennesaw GA) was then used to further emulsify the tumor samples, in short, 10-15 second time intervals, to avoid heating the samples and inadvertently destroying the protein sample. After samples were sufficiently homogenized, the Falcon tubes were tightly sealed and allowed to rock at 4°C for two hours. After two hours, the samples were transferred to 1.5 mL Eppendorf tubes and centrifuged at 10,000 RPM, 4°C for 8 minutes. After spinning, samples

separate into three layers, with the protein extract being contained in the middle layer. The middle layer was transferred to clean 1.5 mL Eppendorf tubes and stored at -80°. Protein concentrations were later determined using the Tecan Infinite M200 PRO microplate reader (Männedorf, SZ).

Lysis Buffer

940uL Lysis Buffer (described below)

10 uL phosphatase inhibitor cocktail 2 (Sigma, St. Louis MO)

10 uL phosphatase inhibitor cocktail 3 (Sigma, St. Louis MO)

40 uL protease inhibitor cocktail (Roche, Basel SZ)

Lysis Buffer

50mM Tris hydrochloride (Sigma Aldrich, St. Louis MO)

150 mM sodium chloride (Sigma Aldrich, St. Louis MO)

1mM ethylenediaminetetraacetic acid (EDTA) (Fisher Scientific, Carlsbad CA)

5% glycerol (Fisher Scientific, Carlsbad CA)

1% Igepal (pH to 7.75) (Sigma Aldrich, St. Louis MO)

J. Cellular Protein Lysates

Mass20 and melanA cells, as described earlier, were grown to 80-90% confluence in 60mm plates. When confluent, each plate was washed using 1mL 1xPBS and cells were collected by mechanical scraping with 200uL of extraction buffer [4x Laemmeli sample buffer (Bio Rad, Hercules CA), 4.7% 2-mercaptoethanol (Sigma, St. Louis MO)]. Extract was transferred to 1.5mL Eppendorf tubes and heated for 10 minutes at 99°C on a

glycerol heat block. After heating, extracts were centrifuged for 10,000 RPM for 10 minutes. After centrifugation, supernatant was collected and stored at -80°.

K. Western Blots

Protein lysates were prepared as described below, and electrophoresed on 10% or 15% SDS gels at 120V for 1.5 hours. For reference, 10uL Bio-Rad protein ladder was loaded into one well per SDS gel. After running, the gel was transferred to a nitrocellulose membrane, at 170mA, in 4° for 3 hours. After transferring, the membrane was stained with Ponceau red dye to visualize the transferred protein, cut to isolate the desired protein size from the remaining portions of the membrane. The cut membrane strips were blocked with 0.25% non-fat dry milk in TBST (Tris buffered saline [1.37 M NaCl, 0.28 M Tris Base (Sigma Aldrich, St. Louis, MO) dissolved in 3L of deionized water, reduced to pH 7.6, and brought to a final volume of 4L] + Tween 20 (Sigma Aldrich, St. Louis MO) on a Snap ID (Millipore, Billerica, MA). Membranes were incubated overnight with primary antibody, diluted with 0.25% non-fat dry milk in TBST. The next day, membranes were washed again with TBST on the SnapID, and incubated with the secondary antibody appropriate for the individual primary antibody, diluted with 0.25% milk for one hour at room temperature, ladder bands were highlighted using WesternSure pen (LI-COR, Lincoln NE) and membranes were incubated in Lumina Crescendo Western HRP substrate (Millipore, Billerica, MA). Chemiluminescent imaging of membranes was achieved using the SynGene GeneGnome. The SynGene GeneSys image capturing system was used to capture images at select time points, as described in the figure legends.

L. Protein Lysate Preparation

Tumor Lysates: Sample dye (5x: 250 mM Tris HCl, 10% SDS, 0.05% bromophenol blue) was diluted to 1x with 85% glycerol and 9.8% 2-mercaptoethanol (Sigma, St. Louis MO). Each sample contained 25 ug of protein lysate and 4uL 1x protein sample dye. A volume of lysis buffer, used in the original extraction was also added to each sample, bringing the final volume to 25uL. Samples were heated for 5 minutes at 95° on a glycerol heat block.

Cellular Lysates: 15uL of each sample was heated for 5 minutes at 95° on a glycerol heat block.

M. Antibodies

I. The Living Colors DsRed polyclonal antibody (Clontech, Mountain View CA) was diluted 1:1000 in 0.25% milk, and used to visualize the band pattern on 29kD membrane sections. After incubating in primary antibody overnight, 29kD membrane sections were exposed to an anti-rabbit secondary antibody and imaged.

II. The γH2AX antibody (Millipore, Billerca MA) was diluted 1:1000 in 0.25% milk, and used to visualize the band pattern on 15kD membrane sections. After incubating in primary antibody overnight, 15kD membrane sections were exposed to an anti-mouse secondary antibody and imaged.

III. The PD-L1 antibody (ProSci, Poway CA) was diluted 1:1000 in 0.25% milk, and used to visualize the band pattern on the 37kD membrane section. After

incubating in primary antibody overnight, 37kD membrane sections were exposed to an anti-rabbit secondary antibody and imaged.

IV. Tubulin monoclonal antibody (Sigma, St. Louis MO), used to quantify total protein, was diluted 1:10,000 in 0.25% milk and used to visualize the band pattern on 50kD membrane sections. After incubating in the primary antibody for fifteen minutes at room temperature, 50kD sections of membrane were exposed to an anti-mouse secondary antibody to visualize the band pattern.

RESULTS

Part I: Injection and treatment protocol optimization

Initially, one aim for this experiment was to monitor tumor development and metastasis to distant organs by utilizing Mass20 cells, a GRM1-positive clone from the Mass population described earlier, expressing red fluorescent protein (RFP). After transfection, RFP-positive cells were selected for using either 0.75ug/mL or 1ug/mL puromycin. Individual clones were confirmed as RFP-positive using Nikon Eclipse Ti fluorescence inverted microscope (Nikon, Tokyo JP) and confirmed by Western blot. To achieve this aim, $1x10^6$ Mass20-RFP cells, suspended in PBS, were injected subcutaneously into the flanks of twenty-seven immunocompetent C57BL/6 mice. For this group of animals, treatment across all groups was initiated one week after injection, independent of tumor growth. After one week of treatment, or two weeks after Mass20-RFP injection, only three animals (11%) had developed palpable tumors. Previous work with Mass clones allografted into C57BL/6 animals showed 100% aggressive tumorigenesis within 5-7 days of injection(17). Based on this prior observation, increased latency seen in this model was unexpected, however, treatment was not discontinued. After two months, post-injection, sixteen animals (59%) still had not developed palpable tumors and the experiment was terminated. Tumors that did develop, were collected during necropsy, and preserved as described earlier. No serum or splenic tissue was collected from these animals.

Based on the first experiment, it was unclear whether the observed reduction to tumorigenicity resulted from injection of a less tumorigenic Mass20-RFP clone or the

early initiation of treatment. For the next group of animals in the second experiment, the parent Mass20 clone was used to inject the flanks of sixty-two C57BL/6 animals, but only $5x10^5$ cells in PBS were used. The number of injected cells was reduced by half to prevent tumors from forming and growing too rapidly, before a sufficient treatment time could be reached. Additionally, treatment was not initiated for this group until tumors were palpable. In this group, only three animals (4.8%) developed tumors within ten days of injection. By two weeks, post-injection, though, fifty-five (88.7%) of animals in this group had developed palpable tumors. Treatment of animals in this group took place over two months after injection of the Mass20 cells, however, very few individuals across all treatment groups could be maintained longer than two weeks after initiation of treatment, due to aggressive tumorigenesis. When animals in this group reached endpoint, tumor tissue was collected from all animals, as well as serum from three representative animals across all treatment groups.

In an effort to strike balance between variable tumorigenicity observed in the first two experiments, we further reduced the number of subcutaneously injected cells to $2x10^5$ per flank and used a mixture of three different clones of RFP-expressing Mass20 in thirty-eight C57BL/6 animals. By combining three clones, we hoped to avoid any questions about reduced tumorigenicity in individual clones, resulting from selection of the exogenous RFP plasmid DNA. We also waited until tumors became palpable before initiating treatment in this group. Within one month of injecting Mass20-RFP mixed clonal cells, only seven animals (18%) had developed palpable tumors. By two months, post-injection, only four additional animals (29%), had

developed palpable tumors. Untreated, non-tumor bearing animals were maintained for four months post-injection to determine if additional time would result in development of more tumors. Some animals developed pigmentation like the dark colored region resulting from Mass20 or Mass20-RFP injection, but these pigmented regions never became raised or palpable, like other tumors arising from injection of these cells. In this group, the proportion of animals where tumor development was observed never reached over 50%. When any treated animal reached a point where sacrifice, due to tumor volume, was necessary, tumor tissue was collected during necropsy. Additionally, blood from three animals, across all treatment groups was collected. Unfortunately, as not all animals developed tumors, serum samples from all time points, across all treatment groups were not obtained.

A fourth group of thirty-eight C57BL/6 animals were injected with a further reduced number (10^5) of parental Mass20 cells in PBS. From this group only fifteen animals (39%) developed palpable tumors and went on to receive treatment. When these few animals reached the tumor volume threshold and sacrifice was required, tumor tissue was collected. Serum was also collected from three representative animals, from each treatment group. However, due to tumorigenicity observed in so few animals, complete sets of serum from all time point could not be obtained from this group of animals.

Part II: Tumor volume measurements & survival

For the next *in vivo* tumorigenicity assessment, Mass20 parent cells were utilized. As described earlier in the methods, $2.5x10^5$ Mass20 cells, mixed with Matrigel basement membrane (Corning, Corning NY) were injected subcutaneously to both flanks of unconscious C57BL/6 animals. Treatment, as described in Figure 4, was initiated when Mass20 tumors became palpable, seven to ten days post-injection. After receiving treatment for four weeks, tumor volumes observed in animals receiving combination therapy, riluzole or FC4157 compound with PD-1 blockade, showed significantly reduced tumor volumes as compared to animals receiving monotherapy treatments or either vehicle treatment (Figure 5). Tumor volumes normalized to day 1, when treatment was initiated and tumors were first measured, further showed the reduced tumor volumes over four weeks in groups receiving combination therapy (Figure 6). As animals receiving combination therapy showed reduced tumor growth, these animals could be maintained slightly longer than animals receiving monotherapy or vehicle treatments (Figure 7). Interestingly, we also observed reduced tumor growth, and consequently, slightly improved survival in animals receiving rat IgG vehicle treatment. Based on individual tumor measurements, some animals could be maintained and treated up to five and a half weeks before tumor volumes reached the threshold where sacrifice was required, per IACUC protocol.

Part III: Western blots using tumor tissue protein lysates

A. Reduced PD-L1 expression in tumors from combination treatment groups

As described earlier, surface expression of PD-L1 on tumor cells can engage the PD-1 receptor on active, cytotoxic CD8+ T cells. Engagement of PD-1 by PD-L1 on tumor cells can prevent detection and subsequent destruction of these tumor cells by cytotoxic CD8+ T cells. To investigate the ability of tumors to evade an immune response through exploitation of PD-1 signaling, as discussed earlier, we extracted protein lysates from tumors collected from animals in all treatment groups. Western blot analysis showed reduced PD-L1 expression in tumors from animals receiving combination therapy, as compared to animals receiving monotherapy or vehicle treatments (Figure 8). Tumors from animals receiving either form of combination therapy reflected PD-L1 expression levels similar to those expressed in cultured nontumorigenic melanA and tumorigenic Mass20 cell lines. Tumors from animals administered FC4157 monotherapy also showed slightly reduced PD-L1 expression, as compared to tumors from animals receiving riluzole monotherapy, αPD-1 monotherapy, or vehicle treatments. Surprisingly, tumors from animals administered αPD-1 antibody monotherapy showed the highest level of PD-L1 expression.

B. Increased γH2AX expression in tumors from combination therapy groups

Our group previously demonstrated an increase in DNA damage marker, γH2AX, as a result of riluzole treatment in *in vitro* cultured cells and *in vivo* animals(28). γH2AX is a phosphorylated histone variant and well-known marker of DNA double-stranded breaks(31). Recent analysis of two independent cohorts revealed patients with

melanoma characterized by a high mutational burden showed improved, durable responses and progression-free survival after undergoing PD-1 inhibition treatment(43). To assess DNA damage acquired within the tumors of animals across current treatment groups, protein lysates were extracted from excised tumors and Western blots probing for γH2AX were performed. As expected, administration of riluzole as part of a combination therapy or monotherapy regimen in our current immunocompetent model yields substantial accumulation of γH2AX. Additionally, the riluzole pro-drug, FC4157, which has not been previously studied to determine its potential to induce DNA damage, also yielded slightly increased levels of γH2AX. Increased levels of γH2AX were detected in protein lysates from tumors collected from animals receiving either riluzole or FC4157 as either a monotherapy or in combination with αPD-1 blockade. In tumors from animals treated with either form of combination therapy, though, the levels of γH2AX detected were higher than the levels observed in tumors from animals receiving either drug as a monotherapy. Levels of γH2AX detected in tumors from animals receiving αPD-1 antibody did not significantly change as compared to lysates from either vehicle treated group (Figure 9), suggesting inclusion of αPD-1 did not further promote DNA damage *in vivo*.

Part IV: Cytokine expression in tumors, spleens, and serum

Cytokines are small proteins that act as molecular messengers, allowing immune cells to communicate and coordinate responses to antigen. These secreted or membrane bound proteins can affect how immune cells behave through regulation of inflammation, immune cell growth and proliferation, DNA repair response, and by altering the tumor microenvironment to be more hospitable or hostile to immune cell activity(44). To better understand how our treatment groups altered the tumor microenvironment and potential for immune response, we used ELISA arrays to analyze cytokine expression patterns in tumor tissue, splenic tissue, and serum from all treatment groups. Analysis was performed using LEGENDPlex Mouse Cytokine Panel 2 (BioLegend, San Diego CA), which determines the concentration, in pg/mL, of cytokines IL-1α, IL-1β, IL-3, IL-7, IL-11, IL-12p40, IL-12p70, IL-23, IL-27, IL-33, IFN-β, GM-CSF and thymic stromal lymphopoietin (TSLP). The role of some cytokines, including IL-1, IL-3, and IL-27, in anti-melanoma responses are still unclear and, for this reason, will not be discussed in detail here. Recent studies suggest expression of IL-23, a cytokine whose role in anti-tumor responses has historically been elusive, plays a crucial role in DNA damage repair within melanocytes(44, 45). Additionally, IL-23 expression in melanoma may also help shift the tumor microenvironment towards a more anti-tumorigenic phenotype, by limiting regulatory T cell infiltration and reducing production of immune-suppressive and inflammatory cytokines like IFNγ and IL-10(45). In our system, IL-23 expression only increases slightly in rat IgG vehicle treatment and combination one therapy groups, in serum and splenic tissue, respectively. In tumor tissue, we see some

increases in the expression of this cytokine in FC4157 monotherapy and combination two treatment groups. However, without similar increases observed in other tissue or serum, it is difficult to infer what role IL-23 is playing in our model. For this reason, implications of IL-23 expression will not be addressed in detail.

A. ELISA array shows differences in cytokine expression between tumor sets

To better understand interactions between the immune system of C57BL/6 animals and implanted Mass20 tumors, we analyzed two sets of tumor tissues, by ELISA arrays. Tumor set one includes tumor tissue from one representative animal from each of the seven treatment groups. Tumor set two includes tissue from one representative animal from each of the treatment groups, except monotherapy FC4157. To determine change in cytokine expression across treatment groups, riluzole and FC4157 data were compared to data from vehicle one, DMSO, αPD-1 data was compared to vehicle two, rat IgG, and data from both combination groups were compared to an average of vehicle one and two data.

Interestingly, data from tumor set one generally shows increases to most assayed cytokines across all treatment, non-vehicle groups, with few exceptions. These exceptions include decreases to IL-12(p70), IL-7, IL-11, IL-33, and IFN-β in αPD-1 treated animals; decreases to IL-11 and IFNβ in combination one treated animals; and decreases to IL-12(p40), IL-7, and IL-11 in combination two individuals. These exceptions made up only 21.5% of assayed cytokines for tumor set one. Conversely, data from tumor set two shows decreases to all assayed cytokines across all treatment groups, with only one

exception; a very minor increase to IL-7 in an animal receiving αPD-1 treatment (Figure 10).

This contrasting data is particularly puzzling, as these sets of tumor tissues were collected within three days of each other. For this reason, data from both tumor sets were averaged and cytokine expression values were normalized to values shown in respective vehicle treatment groups (Figure 11). Based on this analysis, tumor tissue from one animal treated with FC4157 monotherapy showed the greatest number of notable increases to assayed cytokines (46.2%). IL-12 (p70), IL-7, IL-33, and GM-CSF all increased noticeably in this treatment group, as compared to animals treated in the vehicle one group. Unfortunately, as tumor set two lacked tissue from this treatment group, this analysis is only informed by the tissue from a single animal. Like the results observed with FC4157 monotherapy, tumors from animals receiving this treatment as part of the combination two regimen showed obvious increases to two notable cytokines, IL-12 (p70) and TSLP. Tumors from animals in riluzole and αPD-1 monotherapy groups showed notable increases in GM-CSF expression. Animals receiving riluzole as part of combination one therapy did not show distinguishable increases to expression of GM-CSF, but did show increased expression of IL-12 (p70). Determining whether these noticeable increases are significant will require additional analysis of more tumor samples.

B. ELISA array shows increased cytokine expression in spleens from all treatment groups, notably, the combination one group

Splenic tissue collected from the riluzole monotherapy treated group only showed increases to four assayed cytokines (30.7%), IL-12 (p70), IL-7, IL-33, and TSLP (Figure 12). Interestingly, this treatment group showed the lowest proportion of assayed cytokines to increase in expression, while the combination one group, showed the highest proportion (69%). When riluzole and αPD-1 antibody was administered as a combination therapy, samples of splenic tissue showed increased expression of all assayed cytokines except IL-27.

When αPD-1 antibody is administered as a monotherapy, samples of splenic tissue show large increases to IL-12 (p40), IL-7, and IL-33, while more modest increases are seen in IL-12 (p70) and GM-CSF expression. Finally, splenic tissue collected from animals in the combination two group show highly elevated expression of IL-7 and IL-33, as well as mildly enhanced expression of IL-12 (p40), IL-12 (p70), and GM-CSF. Determining whether these increases are significant will require additional analysis of more spleen samples.

C. ELISA array analysis shows increased cytokine expression in serum from αPD-1, rat IgG treatment groups.

To better understand interactions between the immune system of C57BL/6 animals and implanted Mass20 tumors, we analyzed two sets of serum, collected from peripheral blood, by ELISA. A single set of serum included one sample from time point 0 (T0), before injection of Mass20 cells and prior to initiating treatment, and one sample from endpoint, immediately before animals were sacrificed. T0 and endpoint were compared to determine changes in cytokines. Data from both sets at T0 and endpoint

were averaged. Serum samples were run on the same lymphocyte panel used to analyze both sets of tumor tissue, and the single set of splenic tissue. Data showed all treatment groups expressing different cytokine patterns (Figure 13).

Most surprising was the data obtained from animals receiving rat IgG as a vehicle treatment. Serum from animals in these treatment groups showed the highest number of cytokines with increased expression investigated in this assay. Twelve of thirteen cytokines (92%) showed increased expression levels in serum between time point 0 and endpoint. The only cytokine from this group with decreased expression, IL-27, decreased in all treatment groups. Of the cytokines with increased expression in this group, IL-1a and IFNβ were the only two cytokines that did not show percent increases larger than 100% (Figure 14). Conversely but less surprisingly, animals receiving DMSO in the vehicle one treatment group did not show any increased cytokine expression between T0 and endpoint (Figure 13). Serum from animals treated with PD-1 blockade showed the next highest proportion (61%) of cytokines with increased expression after Mass20 cell injection and treatment initiation. For all other treatment groups, between 15-30% of assayed cytokines showed increased expression level between T0 and endpoint.

In serum from animals treated with PD-1 blockade as a monotherapy, levels of IL-3, IL-12(p70), IL-7, IL-11, IL-33, IFNβ, GM-CSF, and TSLP were all elevated at endpoint, as compared with serum collected at time point 0 (Figure 13). IL-3, IL-7, IL-11, and IFNβ all showed percent increases greater than 100% (Figure 14). Serum from animals receiving riluzole monotherapy treatment showed increased levels of IL-11 and IFNβ at

endpoint, but only IL-11 showed a percent increase of more than 100% (Figure 14). Interestingly, animals receiving riluzole with PD-1 blockade showed increased levels of IL-7 and IL-33 only, and both cytokines showed percent increases greater than 100% (Figures 13,14). Animals treated with FC4157 showed increased expression of IL-12(p40). Similarly, animals receiving FC4157 and PD-1 blockade also showed increased levels of IL-12(p40), as well as increases IL-7 expression (Figure 13). While samples from the FC4157 treated group did not show any cytokines with large percent increases, in the combination two treated group IL-1a showed a percent increase of more than 100% (Figure 14). Determining whether these increases are significant will require analysis of serum samples from a larger number of animals.

Part V. Chemokine expression in tumors, spleens, and serum

Chemotactic cytokines, more commonly referred to as chemokines, are responsible for controlling cell migration between tissue and influencing the interactions between cells within tissue. These small, secreted proteins play a primary role in immune cell trafficking but also affect motility and behavior of non-immune cells(46, 47). To better understand how the described monotherapy and combination therapy regimens affect immune cell motility in our model, we analyzed expression levels of chemokines in sets of tumor tissue and spleen tissue. Tumor samples were analyzed using the LEGENDPlex Mouse Proinflammatory Chemokine Panel (BioLegend, San Diego CA), which determined the concentration, in pg/mL, of chemokines CCL2, CCL5, CXCL10, CCL11, CCL17, CCL3, CCL4, CXCL9, CCL20, CXCL5, CXCL1, CXCL13, and CCL22. Splenic tissue and serum samples, both described in later sections, were also analyzed using this panel. Of the chemokines investigated, CXCL10, CXCL9, and CCL4 have been identified for their direct or indirect role in anti-tumor immune responses(46). Conversely, CXCL1, CXCL13, CCL2, CCL3, CCL11, and CCL22 have been identified as chemokines associated with promoting tumor growth, invasiveness, or angiogenesis(46, 47). Finally, chemokines CXCL5, CCL5, CCL17, and CCL20 have been associated with different outcomes in preclinical and clinical investigations and their role in anti-tumor immune responses remains elusive. For this reason, the following results and discussion sections will focus on the chemokines with well understood roles in tumor immunity.

A. ELISA array shows increased chemokine expression in tumors, spleens from monotherapy treatment groups

As compared to samples from the vehicle one group, tumor samples from animals treated with riluzole showed increased levels of CCL11, CCL17, CXCL1, CCL2, CCL3, CCL4, and CLL22 (Figures 15,16). Spleens from the same treatment group similarly showed increased expression of CXCL1, CCL3, and CCL22, and uniquely, CXCL13 (Figure 15). Tumors and spleens from the riluzole treated group showed the largest proportion of increases to chemokines investigated in this assay (Figure 15).

Surprisingly, tumor samples from the combination of riluzole and PD-1 blockade did not reflect a similar chemokine expression pattern. The only chemokine with elevated expression in tumor tissue, compared to vehicle, from this group was CXCL10, and this increase in expression was minor (Figure 16). The data from cytokine expression in the spleen from the combination one group, though, did closely reflect the expression pattern of the spleen from the riluzole group. Like the riluzole group, CXCL1, and CXCL13 showed increased expression the spleen of one animal receiving combination one therapy. Chemokine CCL3 expression was also increased in the spleen collected from an animal treated with combination one therapy (Figure 17).

Like the combination one tumors, the single tumor collected and analyzed from the FC4157 group only showed expression of CXCL10 (Figures 15,16). Unfortunately, no splenic tissue was available from this treatment group. Chemokine expression seen in spleens from animals treated with combination two matched the expression pattern of splenic tissue from combination one exactly, with increases to CXCL1, CCL3, and CXCL13

(Figures 15, 17). Expression pattern of the tumor tissue from this group also showed increased expression levels of CXCL1, as well as elevated CXCL10 expression (Figures 15, 16).

Tumor tissues collected from animals receiving monotherapy PD-1 blockade showed increased expression of CCL17, CXCL1, CCL2, CCL3, and CCL22 (Figures 15, 16). Surprisingly, the splenic tissue from the same treatment group showed most of these cytokines at decreased levels, as compared to the rat IgG vehicle treated group, while CCL3, CXCL13 increased (Figure 17). Determining whether these increases are significant will require analysis of more tumor and spleen samples.

B. ELISA array shows increased chemokine expression in serum from all treatment groups.

Serum samples, as described previously, also underwent analysis to determine changes to chemokine levels between time point 0 and endpoint. Chemokine expression patterns in the serum may help us learn more about immune cell trafficking from immune tissues to the tumor microenvironment.

Sera from animals receiving PD-1 blockade monotherapy had the lowest number of altered cytokines assayed between time point 0 and end point. In this group, only CXCL1, CCL2, and CXCL13 showed increased expression. When PD-1 blockade was combined with FC4157, increases to CXCL1, CCL2, and CXCL13 were also observed, in addition to increases to CCL17. Administration of PD-1 blocking antibody with riluzole led to similar increases of the five chemokines shown to increase with FC4157 and PD-1 blockade combination treatment. In the combination one group, four additional

chemokines, CCL3, CCL4, CXCL9, and CXCL10 also increased in expression levels between the time points. Surprisingly, these same ten chemokines also increased with vehicle one DMSO treatment. It is worth noting that many of the largest percent increases in chemokine expression were also observed in the combination one and vehicle one treatment groups. Finally, a large percent increase in CCL2 expression was observed in sera from animals treated with rat IgG vehicle treatment. Increased expression of chemokines CCL17, CXCL1, CCL4, and CXCL13 was also observed in sera from this treatment group, but the percent increase was less drastic than the increase observed in CCL2 expression (Figure 18).

DISCUSSION

After optimizing treatment schedules and injection methods with previous experiments, preclinical animal data from this study supports the hypothesis that riluzole, or riluzole pro-drug FC4157, used in combination with PD-1 blockade can reduce melanoma tumor volume more effectively than either modality alone. Combination therapies also resulted in slight improvements to survival as compared to monotherapy.

Decreased PD-L1 expression, observed in protein lysates from tumors, prepared from animals receiving combination therapy, indicate these tumors may be more susceptible to cytotoxic immune response. With lower surface expression levels of PD-L1, tumor cells are less likely to engage with PD-1 receptors on CD8+ T cells and diminish the immune response generated by the cytotoxic T cell subset. Conversely, higher levels of PD-L1, observed in tumors from animals receiving monotherapy or vehicle treatments, indicate tumors more likely to engage the PD-1 receptor, possibly reducing the cytotoxic immune response.

Earlier work by Rizvi, et al. has shown an association between tumors with high mutational burdens and improved response to PD-1 blockade, we investigated γH2AX accumulation in our preclinical system(43). Previous work from the Chen lab showed accumulation of γH2AX in Grm1-positive melanocytic cell lines, after *in vitro* or *in vivo* treatment with riluzole(28, 48). As expected, tumors from animals treated with riluzole or riluzole combination therapy show increased levels of γH2AX. Levels of γH2AX associated with FC4157 treatment were previously unknown. Interestingly, tumors from

animals receiving FC4157 as a monotherapy or part of a combination regimen did not accumulate γH2AX as significantly as those receiving riluzole treatment. The γH2AX levels in FC4157 treated tumors, though, were moderately increased relative to αPD-1 monotherapy or vehicle treatment groups.

Increased levels of γH2AX may indicate tumors with higher levels of DNA damage or increased potential to accumulate mutations as part of intrinsic repair mechanisms. By inducing DNA damage, riluzole may sensitize tumors to concurrent treatment with PD-1 inhibition. The potential synergy between riluzole, or riluzole pro-drug, and αPD-1 treatment needs to be further explored.

Chemokine and cytokine analysis can improve our understanding of the relationship between implanted Mass20 tumors and immune responses in our preclinical melanoma model. ELISA array analyses of tumor tissues, splenic tissues and serum from peripheral blood shows expression patterns indicative of a favorable immune response across various treatment groups. As the expression patterns of chemokines and cytokines were highly variable between both tissues and treatment groups, only results indicating widespread changes in expression are discussed in detail.

IL-12, which is produced by many phagocytic innate immune cells upon antigen encounter, acts as a growth factor for activated NK cells and various populations of effector T cells. This cytokine can promote helper CD4+ T cell differentiation and stimulate cytotoxic CD8+ T cell activity(44). In melanoma models where IL-12 was investigated as a therapeutic agent, high doses of the cytokine were implicated in mediating anti-tumor immune responses(49). In our model, IL-12 expression increases

within tumor tissues, splenic tissues, and serum samples, notably in combination groups and slightly in some monotherapy groups. Enhanced IL-12 expression in groups where reduced tumor volumes were also observed, suggests the generation of an anti-tumor immune response.

IL-7 is critical for T cell development and, when used therapeutically, has shown to increase both CD4+ and CD8+ T cell populations(44). Increases to IL-7 expression observed in splenic tissues, sera, and to a lesser extent, in tumor tissue from the FC4157 treated group, may indicate an improved anti-tumor T cell response, particularly when PD-1 blockade is used as a monotherapy or part of a combination therapy.

IL-11 is a pleiotropic cytokine known to enhance proliferation of various cell types, including many immune cells. When tumorigenic murine melanocytes, B78H1, underwent transduction to express IL-11, reduced tumor volumes and enhanced CD4+ and CD8+ T cells infiltration was observed(50). In our model, sera from animals receiving rat IgG, riluzole, or PD-1 blockade all showed large increases in IL-11 expression after Mass20 cell injection and subsequent treatment. Tumor tissue, however, showed only very modest increases in IL-11 expression from the FC4157 monotherapy group. IL-11 expression in spleens and serum samples, but not tumors, may indicate the early stages of an anti-tumor immune response.

IL-33, generally understood as an indicator of tissue damage, is expressed by necrotic epithelial cells, activated innate immune cells, and, in some malignancies, tumor cells(44). While some studies have shown enhanced expression of IL-33 to support tumor growth, other groups have reported this cytokine to enhance anti-tumor

activity, notably in melanoma models(51, 52). As necrotic tissue was characteristic of every Mass20 implanted tumor observed, increased IL-33 expression in tumors, spleens, and sera may be a relevant cytokine for future investigation.

IFN-β is capable of inhibiting melanoma growth and has been suggested to play a role in inducting antigen presentation by DCs to inactive CD8+ cytotoxic T cells. More recent preclinical work has also provided evidence of IFN-β modulating the tumor microenvironment to favor anti-tumor immune responses, by affecting chemokine production of tumor associated macrophages. As a result of differential chemokine patterns upon peritumoral treatment with IFN-β, the ratio of activated cytotoxic CD8+ T to T regulatory cells shifted in favor of the tumor-fighting CD8+ subset(53). In our system, serum from animals receiving rat IgG vehicle, riluzole and αPD-1 monotherapies all showed increased IFN-β expression. Notably, the levels of IFN-β increased most significantly in the αPD-1 treated group, supporting previous results that IFN-β may have synergistic effects when used with this form of checkpoint blockade(53). In tumor tissue, however, expression of IFN-β decreased across all treatment groups and data from splenic tissue for this cytokine was not reliable, so further analysis will be necessary before any conclusions can be reached.

TSLP, whose production can be induced via pro-inflammatory IL-1β, has been implicated in attracting macrophage to the tumor microenvironment and, as a result, potentially promoting metastatic phenotypes in murine models. In our model, riluzole treatment, as either a monotherapy or in combination with PD-1 blockade, resulted in increased TSLP expression in splenic tissues. This pattern was not seen in sera, where

only αPD-1 and rat IgG treatment groups showed an increase in TSLP. Interestingly, the expression patterns of TSLP in tumors did not match either pattern, and only combination two treated tumors showed increases to TSLP. Reduction of TSLP in the tumor microenvironments, particularly, may indicate immune modulation of the tumor microenvironment, favoring anti-tumor responses(54).

Finally, widespread increases to the pleiotropic cytokine GM-CSF in tumors, spleens, and sera collected is notable. GM-CSF has been shown to promote dendritic cell maturation and activation and enhance anti-tumor immune responses in melanoma experimental animal models. In our system, increased GM-CSF expression may suggest the generation of an enhanced immune response, particularly in combination groups where reduced tumor volumes were observed. However, the pleiotropic nature of GM-CSF may also result in enhanced proliferation of immune suppressive cell populations, importantly, MDSCs(44). Enhanced GM-CSF expression in groups where reduced tumor volumes were observed, may suggest GM-CSF functions to enhance the anti-tumor response in this environment.

The chemokine CXCL1 was the only chemokine where increased expression across multiple treatment groups was observed in both tumors and splenic tissues. Increased expression of this chemokine in sera was also observed in every treatment group except riluzole monotherapy. This cytokine has been reported to be expressed by melanoma tumor cells, which may explain some of the increased expression(47). Up-regulation of CXCL1 in various types of cancer, including melanoma, has been shown to constitutively activate NF-kB, causing enhanced angiogenesis and metastatic

potential(55). In our preclinical melanoma model, angiogenesis associated with tumors was frequently observed through the skin and during necropsy. Enhanced expression of this cytokine, suggests the presence of pro-tumor chemokine signaling in our model.

Increased expression of CCL2 and CCL3 across treatment groups may also indicate an immune suppressive environment, which would likely favor tumor cell growth and proliferation(46). CCL2, which can also be expressed by melanoma cells, helps mobilize tumor infiltrating macrophages, a feature that has been associated with development of chemoresistance and therefore, poor prognosis in many types of cancer(46, 47). Macrophages respond to CCL2 by producing CCL3, which helps retain these cells in the tumor microenvironment, enhancing inflammation while compounding immune metabolic and nutritional constraints in the area(46).

Conversely, increases to CXCL9 and CXCL10, observed in the sera of the combination one group and tumors of FC4157 monotherapy and both combination groups, suggest an environment favoring an anti-tumor immune response. Both chemokines have been shown to inhibit angiogenesis and attract immune cell types, like NK, CD4+ helper T, and CD8+ cytotoxic T cells, that are associated with strong anti-tumor immune responses(47). Unfortunately, data for these chemokines from splenic tissues were not reliable. Future studies, especially with highly angiogenic cell types like Mass20, may benefit from looking more closely at changes to these cytokines in response to treatment.

Expression of CCL4 is necessary for recruitment of dendritic cells, which helps to generate an antigen-specific, anti-tumor immune response by presenting antigen to T

cells, thereby activating them. Without CCL4, effector T cell activation and expansion within the tumor microenvironment would be impaired(46). CCL4 expression has also been used as a measure of T cell infiltration in melanoma models(56). In our model, CCL4 expression is elevated in the sera of animals receiving riluzole and FC4157 monotherapies, as well as combination of riluzole and PD-1 blockade. Splenic tissue from animals receiving riluzole and PD-1 blockade monotherapies also shows increased CCL4 expression. Unfortunately, CCL4 expression data from the spleens of animals receiving combination therapy were too unreliable to report. In tumor tissue, though, expression of this cytokine only increased in the riluzole treated group. High expression in the sera and spleens of some treated groups, but in few tumors, suggests an immune response may be generated, but is diminished in the tumor microenvironment.

Recent work has shown CCL22 overexpression in the tumor microenvironment can attract T regulatory cells to the region, likely having a negative effect on immune cells with anti-tumor activity(57). When CCL22 is blocked with type I interferon, migration of regulatory T cells to the tumor microenvironment is inhibited, slowing tumor progression in melanoma preclinical models(58). Additionally, expression of the receptor for CCL22, CCR4, in the brain has been shown to enhance melanoma cell migration to this area, implicating the CCL22-CCR4 axis in development of brain metastases(59). In our model, CCL22 expression in combination treatment groups is reduced, as compared to vehicle or monotherapies. Splenic tissues and sera also show decreased expression of this chemokine across most treatment groups, notably, both combination therapies. Reduction of CCL22, particularly in the tumor tissues, suggests

the tumor microenvironment of these tissues may be more favorable to anti-tumor immune responses.

As the spleen is a secondary lymphoid tissue, it is not surprising that higher expression of many cytokines and chemokines was observed here, as compared to serum or tumor tissues. One surprising aspect though, is chemokines highly expressed in the spleen, like CXCL13, show decreased expression in tumors. Increased chemokine expression in the spleen, may suggest generation of an immune response, while decreased or unchanged expression of chemokines in the tumor microenvironment may suggest the 4-5 week treatment window was too short to generate a global immune response outside primary lymphoid tissues. Additionally, an immune-suppressive tumor microenvironment may also result in decreased chemokine expression in the tumor tissues.

FUTURE DIRECTIONS

We are interested in performing immunohistochemistry staining on formalin-fixed tumor tissues across all treatment groups. By staining for lymphocyte markers like CD45 or CD3, a clearer picture of the interaction between the host immune system and Mass20 tumor may emerge. Determining ratios of T effector: T regulatory cells could also shed light on the cytokine and chemokine analyses discussed previously. We also plan to use the tumor cell protein lysates to investigate if levels of known apoptosis markers, cleaved PARP and caspase 3, differ across treatment groups. If combination therapy does indeed enhance anti-tumor immunity, we would expect to see levels of these apoptosis markers to increase in tumors from the combination treated groups.

Continued work investigating the utility of combining immunotherapy with targeted therapy as a treatment for melanoma may benefit from analysis of a larger number of tissue or serum samples. Additionally, panels exploring cytokines or chemokines associated with immune suppression or tumor proliferation, like IL-10, IFNγ, and CXCL12 could provide more information about pro-tumor signals competing against anti-tumor responses. Taken together, analysis of both pro- and anti- tumor cytokines or chemokines could help determine which signals dominate in the tumor microenvironment. Further, comparing these competing signals across treatment groups could help determine which therapies are most likely to shift the tumor microenvironment towards an anti-tumor response.

Based on this proof of concept study, our lab plans to further explore combining immune checkpoint inhibition with targeted GRM1 therapy. The TG-3 transgenic model,

developed in the Chen lab, was previously crossed with hairless SKH animals, generating the TGS transgenic line (Chen lab, unpublished work). Like the TG-3 parent, hairless TGS animals show similar tumor development and progression, therefore pigmented lesions can be easily detected. Both TG-3 parent and TGS animals feature a functional immune system. These unique characteristics of the TGS model provide an opportunity to replicate this experiment using a preclinical system that more accurately represents melanoma development in human patients. Additionally, the traits of the TGS animals may help to reduce experimental complexity and variability between individuals, which may be introduced during tumor cell inoculation. TGS animals can also be maintained much longer than allograft Mass20 models used for the current study. Increased longevity of the model will allow us to better elucidate the efficacy of combining targeted and immune checkpoint therapies over time, especially as a robust anti-tumor immune response may be generated over a longer period of time than the 4-5 week treatment window allowed using the described allograft preclinical model.

REFERENCES

1. Melanoma Skin Cancer American Cancer Society2016 [updated May 20, 2016; cited 2017]. Available from: http://www.cancer.org/cancer/skincancer-melanoma/detailedguide/skin-cancer-melanoma-detailed-guide-toc
2. Uong A, Zon LI. Melanocytes in development and cancer. J Cell Physiol. 2010;222(1):38-41. doi: 10.1002/jcp.21935. PubMed PMID: 19795394; PMCID: PMC2783760.
3. Sekwon Jang MBA. Treatment of Melanoma CNS Metastases. Cancer Treatment Research. 2016;167:263-79. doi: 10.1007/978-3-319-22539-5_11; PMCID: 26601867.
4. Fife KM, Colman MH, Stevens GN, Firth IC, Moon D, Shannon KF, Harman R, Petersen-Schaefer K, Zacest AC, Besser M, Milton GW, McCarthy WH, Thompson JF. Determinants of outcome in melanoma patients with cerebral metastases. J Clin Oncol. 2004;22(7):1293-300. doi: 10.1200/JCO.2004.08.140. PubMed PMID: 15051777.
5. Soffietti R, Kocher M, Abacioglu UM, Villa S, Fauchon F, Baumert BG, Fariselli L, Tzuk-Shina T, Kortmann RD, Carrie C, Ben Hassel M, Kouri M, Valeinis E, van den Berge D, Mueller RP, Tridello G, Collette L, Bottomley A. A European Organisation for Research and Treatment of Cancer phase III trial of adjuvant whole-brain radiotherapy versus observation in patients with one to three brain metastases from solid tumors after surgical resection or radiosurgery: quality-of-life results. J Clin Oncol. 2013;31(1):65-72. doi: 10.1200/JCO.2011.41.0639. PubMed PMID: 23213105.
6. Yamamoto M, Serizawa T, Shuto T, Akabane A, Higuchi Y, Kawagishi J, Yamanaka K, Sato Y, Jokura H, Yomo S, Nagano O, Kenai H, Moriki A, Suzuki S, Kida Y, Iwai Y, Hayashi M, Onishi H, Gondo M, Sato M, Akimitsu T, Kubo K, Kikuchi Y, Shibasaki T, Goto T, Takanashi M, Mori Y, Takakura K, Saeki N, Kunieda E, Aoyama H, Momoshima S, Tsuchiya K. Stereotactic radiosurgery for patients with multiple brain metastases (JLGK0901): a multi-institutional prospective observational study. Lancet Oncol. 2014;15(4):387-95. doi: 10.1016/S1470-2045(14)70061-0. PubMed PMID: 24621620.
7. Yun Xia YL, Kenneth D. Westover, Jiaming Sun, Hongxiang Chen, Jianming Zhang, David E Fisher. Inhibition of Cell Proliferation in an NRAS Mutant Melanoma Cell Line by Combining Sorafenib and alpha-Mangostin. PLoS One. 2016;11(5). doi: 10.1371/journal.pone.0155217; PMCID: PMC4859503.
8. Paul B. Chapman MD, Axel Hauschild, M.D., Caroline Robert, M.D., Ph.D., John B. Haanen, M.D., Paolo Ascierto, M.D., James Larkin, M.D., Reinhard Dummer, M.D., Claus Garbe, M.D., Alessandro Testori, M.D., Michele Maio, M.D., David Hogg, M.D., Paul Lorigan, M.D., Celeste Lebbe, M.D., Thomas Jouary, M.D., Dirk Schadendorf, M.D., Antoni Ribas, M.D., Steven J. O'Day, M.D., Jeffrey A. Sosman, M.D., John M. Kirkwood, M.D., Alexander M.M. Eggermont, M.D., Ph.D., Brigitte Dreno, M.D., Ph.D., Keith Nolop, M.D., Jiang Li, Ph.D., Betty Nelson, M.A., Jeannie Hou, M.D., Richard J. Lee, M.D., Keith T. Flaherty, M.D., and Grant A. McArthur, M.B., B.S., Ph.D. Improved Survival with Vemurafenib in Melanoma with BRAF V600E Mutation. New England Journal of Medicine. 2011;364:2507-16. doi: 10.1056/NEJMoa1103782.
9. Reinhard Dummer SMG, Christian P. Turtschi, Nina B. Eggmann, Olivier Michielin, Lada Mitchell, Luisa Veronese, Paul Rene Hilfiker, Lea Felderer, Jeannine D.

Rinderknecht. Vermurafenib in patients with BRAFV600E mutation-positive melnaoma with symptomatic brain metastases: Final results of an open-label pilot study. European Journal of Cancer. 2014;50(3):611-21. doi: http://dx.doi.org/10.1016/j.ejca.2013.11.002.
10. Kleffel S, Posch C, Barthel SR, Mueller H, Schlapbach C, Guenova E, Elco CP, Lee N, Juneja VR, Zhan Q, Lian CG, Thomi R, Hoetzenecker W, Cozzio A, Dummer R, Mihm MC, Jr., Flaherty KT, Frank MH, Murphy GF, Sharpe AH, Kupper TS, Schatton T. Melanoma Cell-Intrinsic PD-1 Receptor Functions Promote Tumor Growth. Cell. 2015;162(6):1242-56. Epub 2015/09/12. doi: 10.1016/j.cell.2015.08.052. PubMed PMID: 26359984; PMCID: PMC4700833.
11. Rosenberg SA, Lotze MT, Muul LM, Leitman S, Chang AE, Ettinghausen SE, Matory YL, Skibber JM, Shiloni E, Vetto JT, et al. Observations on the systemic administration of autologous lymphokine-activated killer cells and recombinant interleukin-2 to patients with metastatic cancer. N Engl J Med. 1985;313(23):1485-92. Epub 1985/12/05. doi: 10.1056/NEJM198512053132327. PubMed PMID: 3903508.
12. Atkins MB, Lotze MT, Dutcher JP, Fisher RI, Weiss G, Margolin K, Abrams J, Sznol M, Parkinson D, Hawkins M, Paradise C, Kunkel L, Rosenberg SA. High-dose recombinant interleukin 2 therapy for patients with metastatic melanoma: analysis of 270 patients treated between 1985 and 1993. J Clin Oncol. 1999;17(7):2105-16. Epub 1999/11/24. doi: 10.1200/JCO.1999.17.7.2105. PubMed PMID: 10561265.
13. Amin A, White RL, Jr. High-dose interleukin-2: is it still indicated for melanoma and RCC in an era of targeted therapies? Oncology (Williston Park). 2013;27(7):680-91. Epub 2013/08/28. PubMed PMID: 23977763.
14. Andtbacka RH, Kaufman HL, Collichio F, Amatruda T, Senzer N, Chesney J, Delman KA, Spitler LE, Puzanov I, Agarwala SS, Milhem M, Cranmer L, Curti B, Lewis K, Ross M, Guthrie T, Linette GP, Daniels GA, Harrington K, Middleton MR, Miller WH, Jr., Zager JS, Ye Y, Yao B, Li A, Doleman S, VanderWalde A, Gansert J, Coffin RS. Talimogene Laherparepvec Improves Durable Response Rate in Patients With Advanced Melanoma. J Clin Oncol. 2015;33(25):2780-8. Epub 2015/05/28. doi: 10.1200/JCO.2014.58.3377. PubMed PMID: 26014293.
15. Fountzilas C, Patel S, Mahalingam D. Review: Oncolytic Virotherapy, updates and future directions. Oncotarget. 2017. Epub 2017/06/15. doi: 10.18632/oncotarget.18309. PubMed PMID: 28611307.
16. Swann JB, Smyth MJ. Immune surveillance of tumors. J Clin Invest. 2007;117(5):1137-46. Epub 2007/05/04. doi: 10.1172/JCI31405. PubMed PMID: 17476343; PMCID: PMC1857231.
17. Jessica L. F. Teh SC. Glutamatergic signaling in cellular transformation. Pigment Cell and Melanoma Research. 2012;25(3):331-42. doi: 10.1111/j.1755-148X.2011.00983.x.
18. Frati C, Marchese C, Fisichella G, Copani A, Nasca MR, Storto M, Nicoletti F. Expression of functional mGlu5 metabotropic glutamate receptors in human melanocytes. J Cell Physiol. 2000;183(3):364-72. Epub 2000/05/08. doi: 10.1002/(SICI)1097-4652(200006)183:3<364::AID-JCP9>3.0.CO;2-X. PubMed PMID: 10797311.

19. Pamela M. Pollock KC-S, Raman Sood, Jin Namkoong, Jeffrey J. Martino, Aruna Koganti, Hua Zhu, Christiane Robbins, Izabela Makalowska, Seung-Shick Shin, Yari Marin, Kathleen G. Roberts, Laura M. Yudt, Amy Chen, Jun Cheng, Arturo Incao, Heather W. Pinkett, Christopher L Graham, Karen Dunn, Steven M. Crespo-Carbone, Kerine R. Mackason, Kevin B. Ryan, Daniel Sinsimer, James Goydos, Kenneth R. Reuhl, Michael Eckhaus, Paul S. Meltzer, William J. Pavan, Jeffrey M. Trent & Suzie Chen. Melanoma mouse model implicates metabotropic glutamate signaling in melanocytic neoplasia. Nature Genetics. 2003;34:108-12. doi: 10.1038/ng1148.
20. Shin SS, Namkoong J, Wall BA, Gleason R, Lee HJ, Chen S. Oncogenic activities of metabotropic glutamate receptor 1 (Grm1) in melanocyte transformation. Pigment Cell Melanoma Res. 2008;21(3):368-78. Epub 2008/04/26. doi: 10.1111/j.1755-148X.2008.00452.x. PubMed PMID: 18435704; PMCID: PMC2854004.
21. Yu LJ, Wall BA, Chen S. The current management of brain metastasis in melanoma: a focus on riluzole. Expert Rev Neurother. 2015;15(7):779-92. Epub 2015/06/21. doi: 10.1586/14737175.2015.1055321. PubMed PMID: 26092602.
22. Hermans E, Challiss RA. Structural, signalling and regulatory properties of the group I metabotropic glutamate receptors: prototypic family C G-protein-coupled receptors. Biochem J. 2001;359(Pt 3):465-84. Epub 2001/10/24. PubMed PMID: 11672421; PMCID: PMC1222168.
23. A D. The pharmacology and mechanism of action of riluzole. Neurology. 1996;47:S233-S41; PMCID: 8959995.
24. Carbone M, Duty S, Rattray M. Riluzole elevates GLT-1 activity and levels in striatal astrocytes. Neurochem Int. 2012;60(1):31-8. Epub 2011/11/15. doi: 10.1016/j.neuint.2011.10.017. PubMed PMID: 22080156; PMCID: PMC3430367.
25. Lin CL, Kong Q, Cuny GD, Glicksman MA. Glutamate transporter EAAT2: a new target for the treatment of neurodegenerative diseases. Future Med Chem. 2012;4(13):1689-700. Epub 2012/08/29. doi: 10.4155/fmc.12.122. PubMed PMID: 22924507; PMCID: PMC3580837.
26. Namkoong J, Shin SS, Lee HJ, Marin YE, Wall BA, Goydos JS, Chen S. Metabotropic glutamate receptor 1 and glutamate signaling in human melanoma. Cancer Res. 2007;67(5):2298-305. Epub 2007/03/03. doi: 10.1158/0008-5472.CAN-06-3665. PubMed PMID: 17332361.
27. Gelb T, Hathaway HA, Wroblewski JT. Triple threat treatment: Exploiting the dependence receptor properties of metabotropic glutamate receptor 1 against melanoma. Mol Cell Oncol. 2014;1(4):e969163. Epub 2014/10/01. doi: 10.4161/23723548.2014.969163. PubMed PMID: 27308372; PMCID: PMC4905213.
28. Wall BA, Wangari-Talbot J, Shin SS, Schiff D, Sierra J, Yu LJ, Khan A, Haffty B, Goydos JS, Chen S. Disruption of GRM1-mediated signalling using riluzole results in DNA damage in melanoma cells. Pigment Cell Melanoma Res. 2014;27(2):263-74. Epub 2013/12/18. doi: 10.1111/pcmr.12207. PubMed PMID: 24330389; PMCID: PMC3947419.
29. Yip D, Le MN, Chan JL, Lee JH, Mehnert JA, Yudd A, Kempf J, Shih WJ, Chen S, Goydos JS. A phase 0 trial of riluzole in patients with resectable stage III and IV

melanoma. Clin Cancer Res. 2009;15(11):3896-902. Epub 2009/05/22. doi: 10.1158/1078-0432.CCR-08-3303. PubMed PMID: 19458050; PMCID: PMC2812866.
30. Mehnert JM, Lee JH, Shirk J, Bhavsar D, Anosike O, Chan JL, Shih W, Chen S, Goydos JS. A phase II trial of riluzole, an antagonist of metabotropic glutamate receptor 1 (GRM1) signaling, in metastatic melanoma. Journal of Clinical Oncology. 2010;28(15_suppl):TPS309-TPS. doi: doi:10.1200/jco.2010.28.15_suppl.tps309.
31. Wall BA, Yu LJ, Khan A, Haffty B, Goydos JS, Chen S. Riluzole is a radio-sensitizing agent in an in vivo model of brain metastasis derived from GRM1 expressing human melanoma cells. Pigment Cell Melanoma Res. 2015;28(1):105-9. Epub 2014/11/05. doi: 10.1111/pcmr.12327. PubMed PMID: 25363352.
32. Rosenberg SA, Niglio SA, Salehomoum N, Chan JL, Jeong BS, Wen Y, Li J, Fukui J, Chen S, Shin SS, Goydos JS. Targeting Glutamatergic Signaling and the PI3 Kinase Pathway to Halt Melanoma Progression. Transl Oncol. 2015;8(1):1-9. Epub 2015/03/10. doi: 10.1016/j.tranon.2014.11.001. PubMed PMID: 25749171; PMCID: PMC4350641.
33. McDonnell ME, Vera MD, Blass BE, Pelletier JC, King RC, Fernandez-Metzler C, Smith GR, Wrobel J, Chen S, Wall BA, Reitz AB. Riluzole prodrugs for melanoma and ALS: design, synthesis, and in vitro metabolic profiling. Bioorg Med Chem. 2012;20(18):5642-8. doi: 10.1016/j.bmc.2012.07.004. PubMed PMID: 22892214; PMCID: PMC3495316.
34. Murphy K, Weaver C. Janeway's immunobiology2017.
35. Pardoll DM. The blockade of immune checkpoints in cancer immunotherapy. Nat Rev Cancer. 2012;12(4):252-64. Epub 2012/03/23. doi: 10.1038/nrc3239. PubMed PMID: 22437870; PMCID: PMC4856023.
36. Linsley PS, Brady W, Grosmaire L, Aruffo A, Damle NK, Ledbetter JA. Binding of the B cell activation antigen B7 to CD28 costimulates T cell proliferation and interleukin 2 mRNA accumulation. J Exp Med. 1991;173(3):721-30. Epub 1991/03/01. PubMed PMID: 1847722; PMCID: PMC2118836.
37. Chen L. Co-inhibitory molecules of the B7-CD28 family in the control of T-cell immunity. Nat Rev Immunol. 2004;4(5):336-47. Epub 2004/05/04. doi: 10.1038/nri1349. PubMed PMID: 15122199.
38. Curran MA, Montalvo W, Yagita H, Allison JP. PD-1 and CTLA-4 combination blockade expands infiltrating T cells and reduces regulatory T and myeloid cells within B16 melanoma tumors. Proc Natl Acad Sci U S A. 2010;107(9):4275-80. Epub 2010/02/18. doi: 10.1073/pnas.0915174107. PubMed PMID: 20160101; PMCID: PMC2840093.
39. Ott PA, Hodi FS, Robert C. CTLA-4 and PD-1/PD-L1 blockade: new immunotherapeutic modalities with durable clinical benefit in melanoma patients. Clin Cancer Res. 2013;19(19):5300-9. Epub 2013/10/04. doi: 10.1158/1078-0432.CCR-13-0143. PubMed PMID: 24089443.
40. Anderson KG, Stromnes IM, Greenberg PD. Obstacles Posed by the Tumor Microenvironment to T cell Activity: A Case for Synergistic Therapies. Cancer Cell. 2017;31(3):311-25. Epub 2017/03/16. doi: 10.1016/j.ccell.2017.02.008. PubMed PMID: 28292435; PMCID: PMC5423788.
41. Alexander W. The Checkpoint Immunotherapy Revolution: What Started as a Trickle Has Become a Flood, Despite Some Daunting Adverse Effects; New Drugs,

Indications, and Combinations Continue to Emerge. P T. 2016;41(3):185-91. Epub 2016/03/10. PubMed PMID: 26957887; PMCID: PMC4771089.
42. Robert C, Schachter J, Long GV, Arance A, Grob JJ, Mortier L, Daud A, Carlino MS, McNeil C, Lotem M, Larkin J, Lorigan P, Neyns B, Blank CU, Hamid O, Mateus C, Shapira-Frommer R, Kosh M, Zhou H, Ibrahim N, Ebbinghaus S, Ribas A, investigators K-. Pembrolizumab versus Ipilimumab in Advanced Melanoma. N Engl J Med. 2015;372(26):2521-32. Epub 2015/04/22. doi: 10.1056/NEJMoa1503093. PubMed PMID: 25891173.
43. Rizvi NA, Hellmann MD, Snyder A, Kvistborg P, Makarov V, Havel JJ, Lee W, Yuan J, Wong P, Ho TS, Miller ML, Rekhtman N, Moreira AL, Ibrahim F, Bruggeman C, Gasmi B, Zappasodi R, Maeda Y, Sander C, Garon EB, Merghoub T, Wolchok JD, Schumacher TN, Chan TA. Cancer immunology. Mutational landscape determines sensitivity to PD-1 blockade in non-small cell lung cancer. Science. 2015;348(6230):124-8. Epub 2015/03/15. doi: 10.1126/science.aaa1348. PubMed PMID: 25765070; PMCID: PMC4993154.
44. Lee S, Margolin K. Cytokines in cancer immunotherapy. Cancers (Basel). 2011;3(4):3856-93. Epub 2011/01/01. doi: 10.3390/cancers3043856. PubMed PMID: 24213115; PMCID: PMC3763400.
45. Nasti TH, Cochran JB, Vachhani RV, McKay K, Tsuruta Y, Athar M, Timares L, Elmets CA. IL-23 Inhibits Melanoma Development by Augmenting DNA Repair and Modulating T Cell Subpopulations. J Immunol. 2017;198(2):950-61. Epub 2016/12/23. doi: 10.4049/jimmunol.1601455. PubMed PMID: 28003381; PMCID: PMC5225020.
46. Nagarsheth N, Wicha MS, Zou W. Chemokines in the cancer microenvironment and their relevance in cancer immunotherapy. Nat Rev Immunol. 2017. Epub 2017/05/31. doi: 10.1038/nri.2017.49. PubMed PMID: 28555670.
47. Chow MT, Luster AD. Chemokines in cancer. Cancer Immunol Res. 2014;2(12):1125-31. Epub 2014/12/07. doi: 10.1158/2326-6066.CIR-14-0160. PubMed PMID: 25480554; PMCID: PMC4258879.
48. Khan AJ, Wall B, Ahlawat S, Green C, Schiff D, Mehnert JM, Goydos JS, Chen S, Haffty BG. Riluzole enhances ionizing radiation-induced cytotoxicity in human melanoma cells that ectopically express metabotropic glutamate receptor 1 in vitro and in vivo. Clin Cancer Res. 2011;17(7):1807-14. Epub 2011/02/18. doi: 10.1158/1078-0432.CCR-10-1276. PubMed PMID: 21325066; PMCID: PMC3070864.
49. Kawamura T, Takeda K, Mendiratta SK, Kawamura H, Van Kaer L, Yagita H, Abo T, Okumura K. Critical role of NK1+ T cells in IL-12-induced immune responses in vivo. J Immunol. 1998;160(1):16-9. Epub 1998/04/29. PubMed PMID: 9551949.
50. Dams-Kozlowska H, Izycki D, Mackiewicz A. IL-11 is a potent anti-melanoma factor. Adv Exp Med Biol. 2001;495:373-7. Epub 2002/01/05. PubMed PMID: 11774596.
51. Jovanovic IP, Pejnovic NN, Radosavljevic GD, Arsenijevic NN, Lukic ML. IL-33/ST2 axis in innate and acquired immunity to tumors. Oncoimmunology. 2012;1(2):229-31. Epub 2012/06/22. doi: 10.4161/onci.1.2.18131. PubMed PMID: 22720252; PMCID: PMC3376988.
52. Gao X, Wang X, Yang Q, Zhao X, Wen W, Li G, Lu J, Qin W, Qi Y, Xie F, Jiang J, Wu C, Zhang X, Chen X, Turnquist H, Zhu Y, Lu B. Tumoral expression of IL-33 inhibits tumor

growth and modifies the tumor microenvironment through CD8+ T and NK cells. J Immunol. 2015;194(1):438-45. Epub 2014/11/28. doi: 10.4049/jimmunol.1401344. PubMed PMID: 25429071; PMCID: PMC4272901.
53. Kakizaki A, Fujimura T, Furudate S, Kambayashi Y, Yamauchi T, Yagita H, Aiba S. Immunomodulatory effect of peritumorally administered interferon-beta on melanoma through tumor-associated macrophages. Oncoimmunology. 2015;4(11):e1047584. Epub 2015/10/10. doi: 10.1080/2162402X.2015.1047584. PubMed PMID: 26451326; PMCID: PMC4589056.
54. Otsuka A DR, Contassot E, French LE. M2 macrophages and innate lymphoid type 2 cells promote metastasis in malignant melanoma via IL-1B-driven thymic stromal lyphopoietin. Journal of Dermatological Science. 2016;84(1):e72. Epub October 2016.
55. Dhawan P, Richmond A. Role of CXCL1 in tumorigenesis of melanoma. J Leukoc Biol. 2002;72(1):9-18. Epub 2002/07/09. PubMed PMID: 12101257; PMCID: PMC2668262.
56. Harlin H, Meng Y, Peterson AC, Zha Y, Tretiakova M, Slingluff C, McKee M, Gajewski TF. Chemokine expression in melanoma metastases associated with CD8+ T-cell recruitment. Cancer Res. 2009;69(7):3077-85. Epub 2009/03/19. doi: 10.1158/0008-5472.CAN-08-2281. PubMed PMID: 19293190; PMCID: PMC3886718.
57. Klarquist J, Tobin K, Farhangi Oskuei P, Henning SW, Fernandez MF, Dellacecca ER, Navarro FC, Eby JM, Chatterjee S, Mehrotra S, Clark JI, Le Poole IC. Ccl22 Diverts T Regulatory Cells and Controls the Growth of Melanoma. Cancer Res. 2016;76(21):6230-40. Epub 2016/11/03. doi: 10.1158/0008-5472.CAN-16-0618. PubMed PMID: 27634754; PMCID: PMC5242486.
58. Anz D, Rapp M, Eiber S, Koelzer VH, Thaler R, Haubner S, Knott M, Nagel S, Golic M, Wiedemann GM, Bauernfeind F, Wurzenberger C, Hornung V, Scholz C, Mayr D, Rothenfusser S, Endres S, Bourquin C. Suppression of intratumoral CCL22 by type i interferon inhibits migration of regulatory T cells and blocks cancer progression. Cancer Res. 2015;75(21):4483-93. Epub 2015/10/04. doi: 10.1158/0008-5472.CAN-14-3499. PubMed PMID: 26432403.
59. Klein A, Sagi-Assif O, Meshel T, Telerman A, Izraely S, Ben-Menachem S, Bayry J, Marzese DM, Ohe S, Hoon DSB, Erez N, Witz IP. CCR4 is a determinant of melanoma brain metastasis. Oncotarget. 2017;8(19):31079-91. Epub 2017/04/19. doi: 10.18632/oncotarget.16076. PubMed PMID: 28415693; PMCID: PMC5458190.

FIGURES

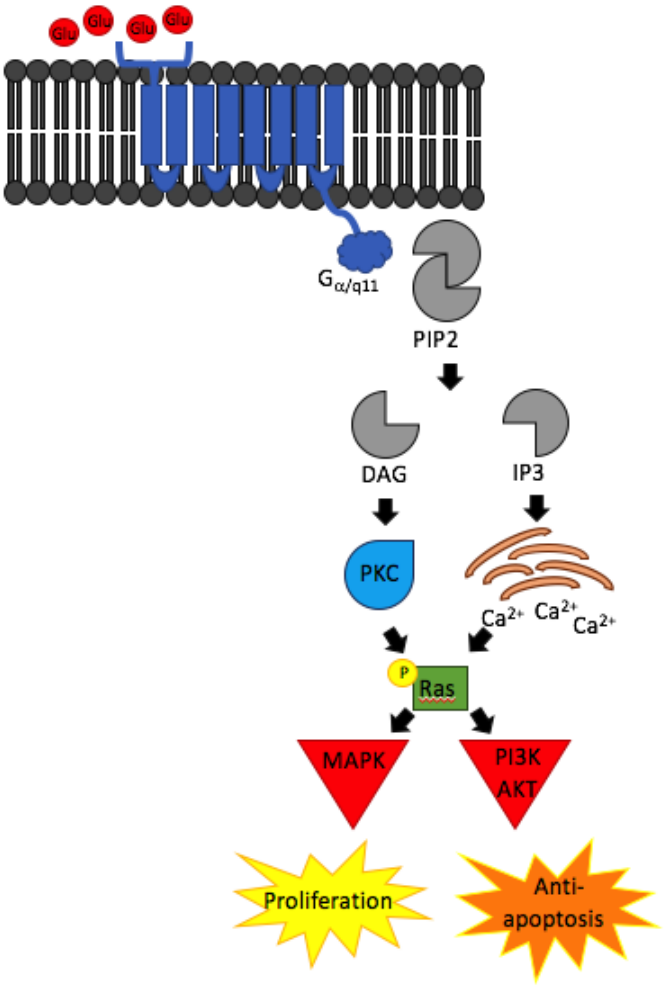

Adapted from Teh and Chen, 2012

Figure 1. Signaling through mGluR1 promotes proliferation and generates anti-apoptotic signals.

When the seven-transmembrane receptor mGluR1 is aberrantly expressed on melanocytes, binding of the natural ligand, glutamate, induces downstream signaling. The receptor couples to G-protein subunits, which causes hydrolysis of PIP2, generating the second messengers DAG and IP3. Individually, these second messengers activate the MAPK and PI3K/AKT signaling cascades, promoting cell proliferation and inhibiting apoptosis, respectively.

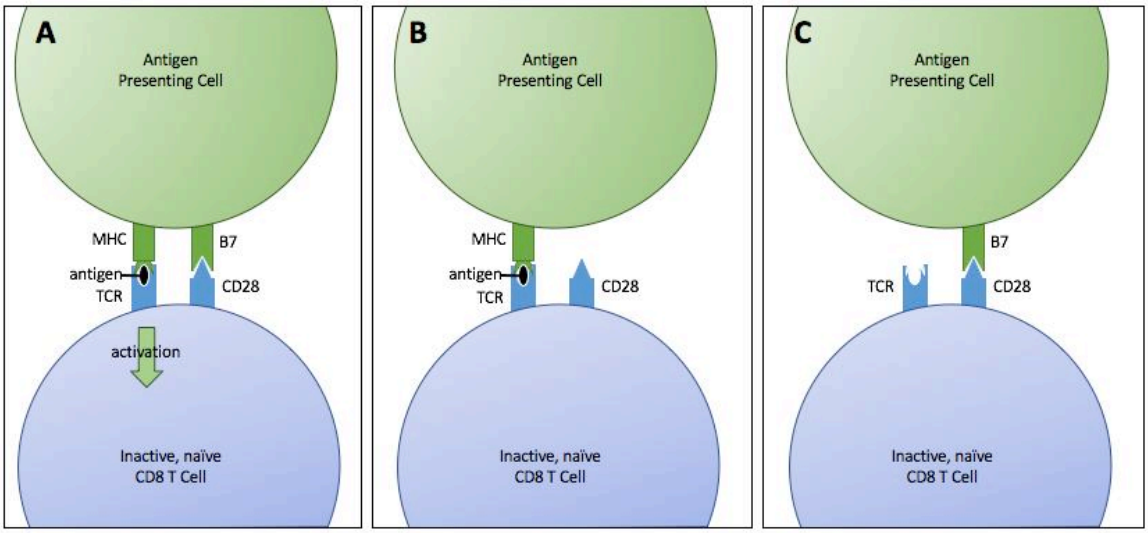

Adapted from Chen, 2004

Figure 2. Optimal T cell activation requires antigen presentation and co-stimulatory signals.

Antigen presenting cells present tumor or foreign antigen on MHC and, under some conditions, express B7 co-stimulatory molecules on the cell surface. Inactive, naïve CD8+ T cells express the TCR, which binds antigen, and CD28, which can engage with B7 on APCs. **A.** When TCR recognizes self-MHC: antigen complex and CD28 engages with B7, intracellular signals allow for activation of the T cell. **B.** When TCR recognizes self-MHC: antigen complex, but the T cell does not receive a co-stimulatory signal from CD28:B7 engagement, no T cell activation is achieved. **C.** Without recognition of self-MHC: antigen complex, no T cell activation is achieved, regardless of CD28:B7 engagement.

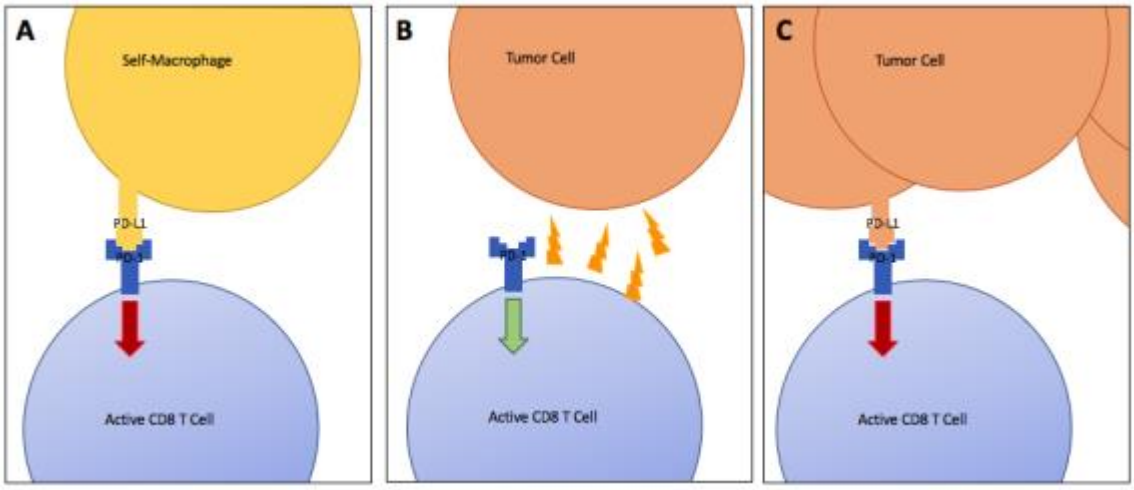

Figure 3. PD-1 engagement by ligand PD-L1 allows T cells to distinguish between normal cells and harmful or foreign cells.
PD-1 is upregulated on the surface of activated T cells in the peripheral tissues. **A.** When normal cells, including many immune cells, endothelial and epithelial cells, express PD-L1, the ligand engages with PD-1 on the surface of T cells, generating inhibitory signals within the T cell, preventing a cytotoxic response. **B.** When an activated T cell encounters a tumor cell that does not express PD-L1, lack of PD-1 engagement on the T cell surface, generates stimulatory signals within the T cell and a cytotoxic immune response against the tumor cell is generated. **C.** When tumor cells express PD-L1, the ligand can engage with PD-1 on the T cell surface, preventing a cytotoxic immune response and allowing tumor cells to survive and proliferate.

DMSO – Vehicle 1		**Daily, oral gavage**
Rat IgG – Vehicle 2	**100ug**	**Intraperitoneal (IP) injection, week 1 3x, then 1x weekly**
Riluzole	**10mg/kg**	**Daily, oral gavage**
αPD-1	**100ug**	**IP injection, week 1 3x, then 1x weekly**
FC4157	**1.7mg/kg**	**Daily, oral gavage**
Riluzole + αPD-1 (Combination 1)	**As described above**	**Both, as described above**
FC4157 + αPD-1 (Combination 2)	**As described above**	**Both, as described above**

Figure 4. Treatment schedule and drug concentrations administered to each treatment group.

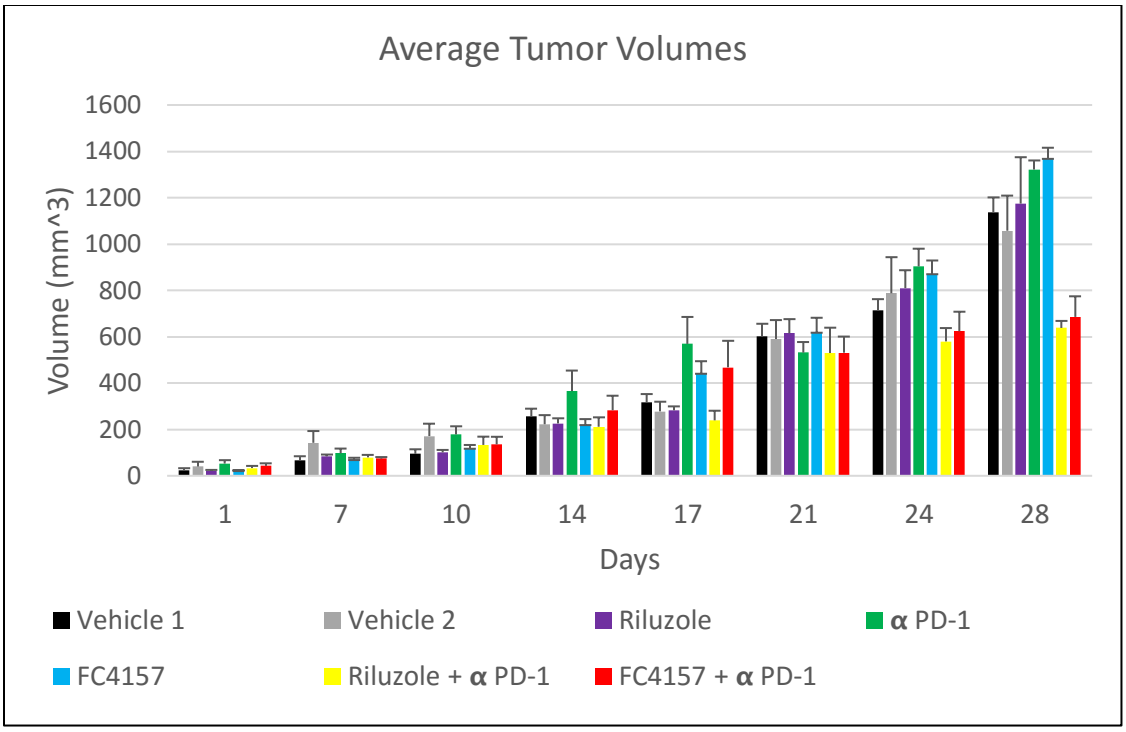

Figure 5. Tumor volumes in C57BL/6 animals, injected with $2.5x10^5$ Mass20 cells, after four weeks of treatment

Tumors were measured twice/week using a Vernier caliper. Average tumor volumes from each treatment group are shown. Tumor volumes from individuals within a treatment group were aligned to a standard time point 1, when tumors were first measured and treatment began.

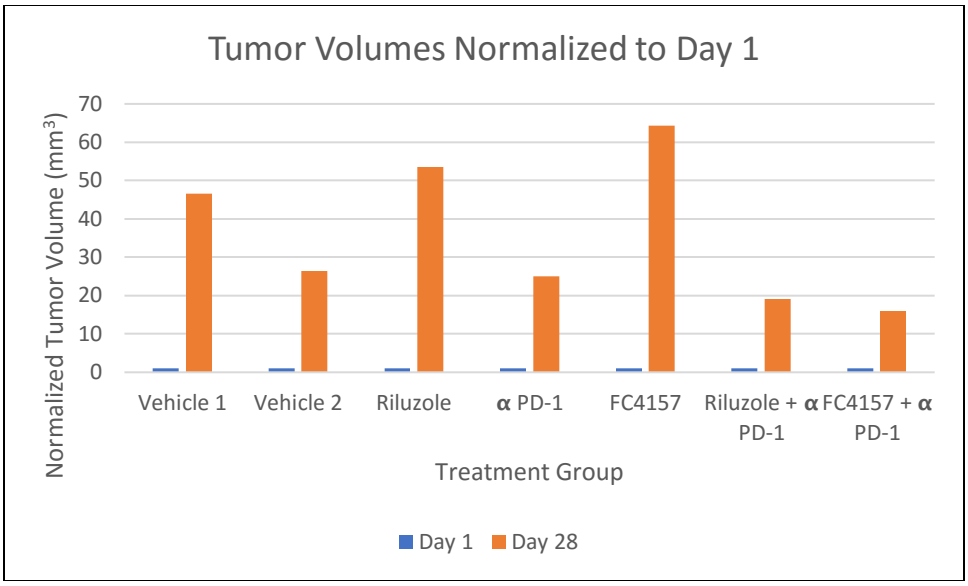

Figure 6. Average tumor volumes, by group, normalized to tumor volume at day 1. As tumor volumes varied slightly between groups at day 1, tumor volumes at day 28, were normalized to day 1. Change to average tumor volume from day 1 to day 28 are shown.

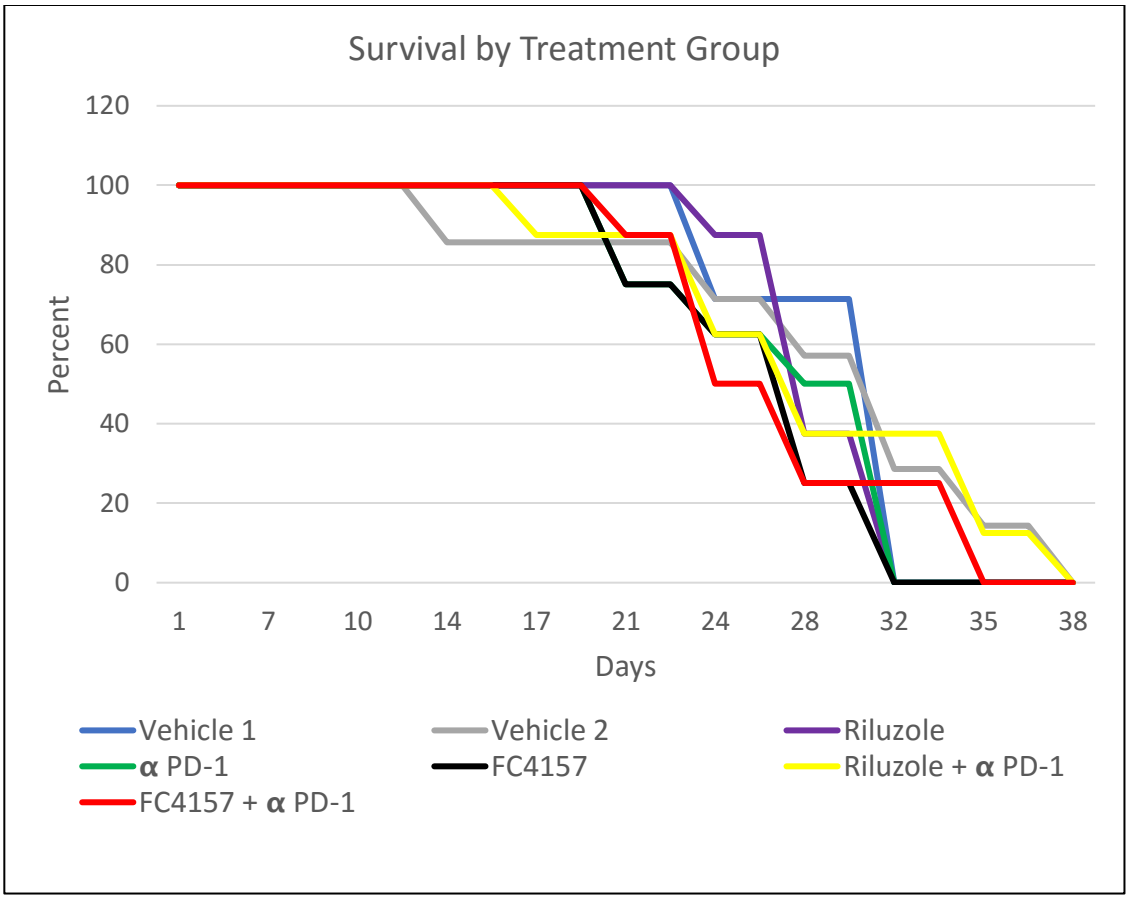

Figure 7. Survival by treatment group, based on tumor volumes.
Per the Chen lab animal protocol, as approved by the Institutional Animal Care and Use Committee and Rutgers University, animals with tumor volumes larger than 1500mm^3 were sacrificed. Animals with tumors less than this threshold could be maintained and treated until the tumor volume threshold was reached.

A

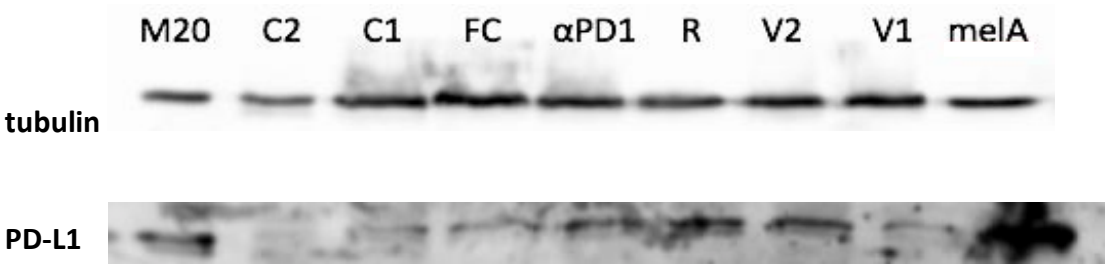

B

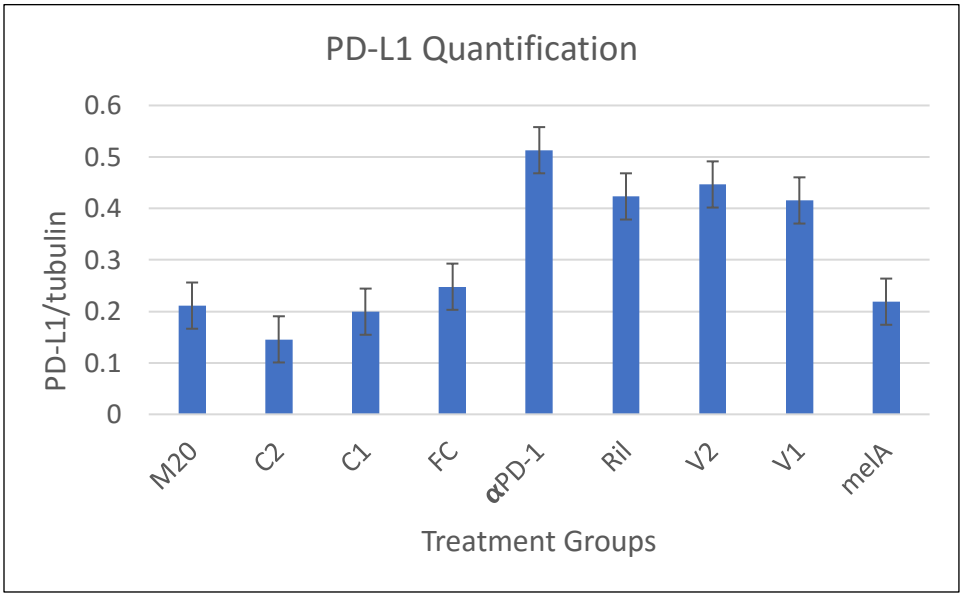

Figure 8. Reduced PD-L1 expression in protein lysates from tumor tissue from combination one and two treatment groups.

Protein lysates were prepared from flash frozen tumors, collected from animals during necropsy, and Western immunoblots of PD-L1 were performed. Lysates from melanA and Mass20 cultured cells were used as controls.

A

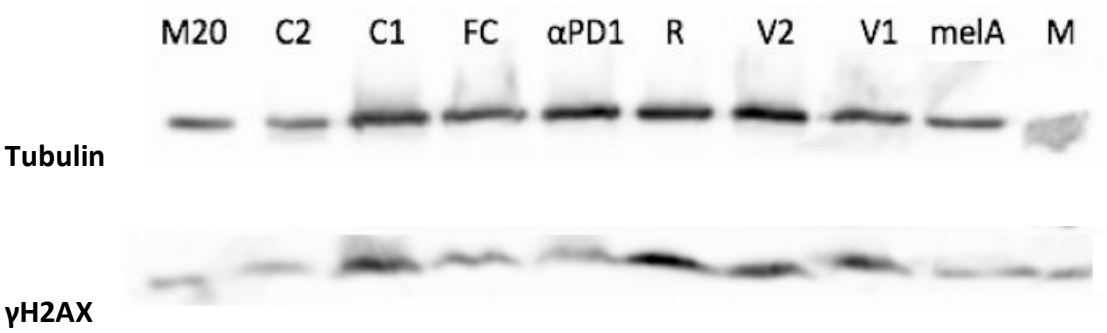

B

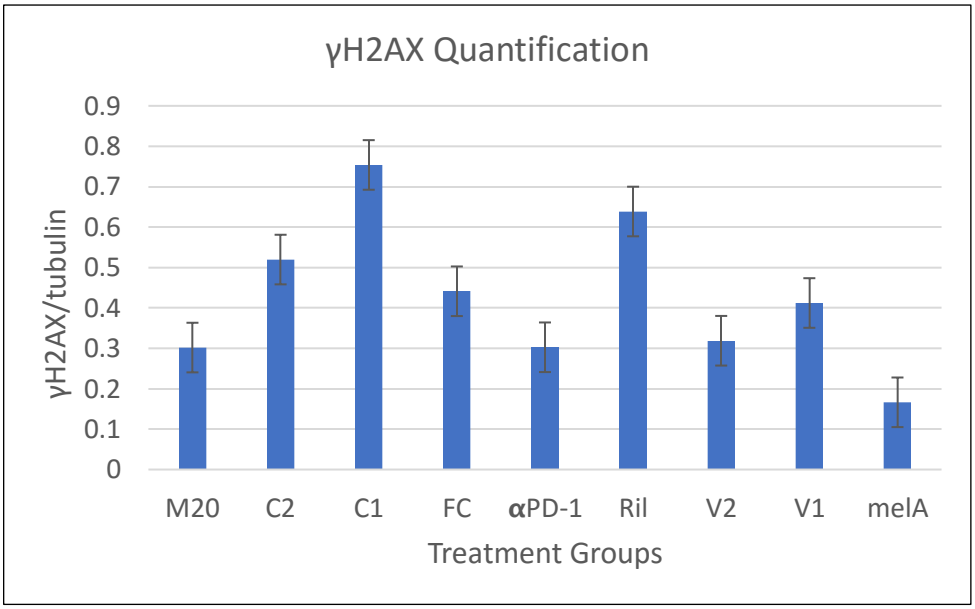

Figure 9. Increased γH2AX expression in protein lysates from tumors developed on animals treated with riluzole and FC4157, as either a monotherapy or part of a combination therapy with PD-1 blockade.

Protein lysates were prepared from flash frozen tumors, collected from animals during necropsy, and Western immunoblots of γH2AX were performed. Lysates from melanA and Mass20 cultured cells were used as controls.

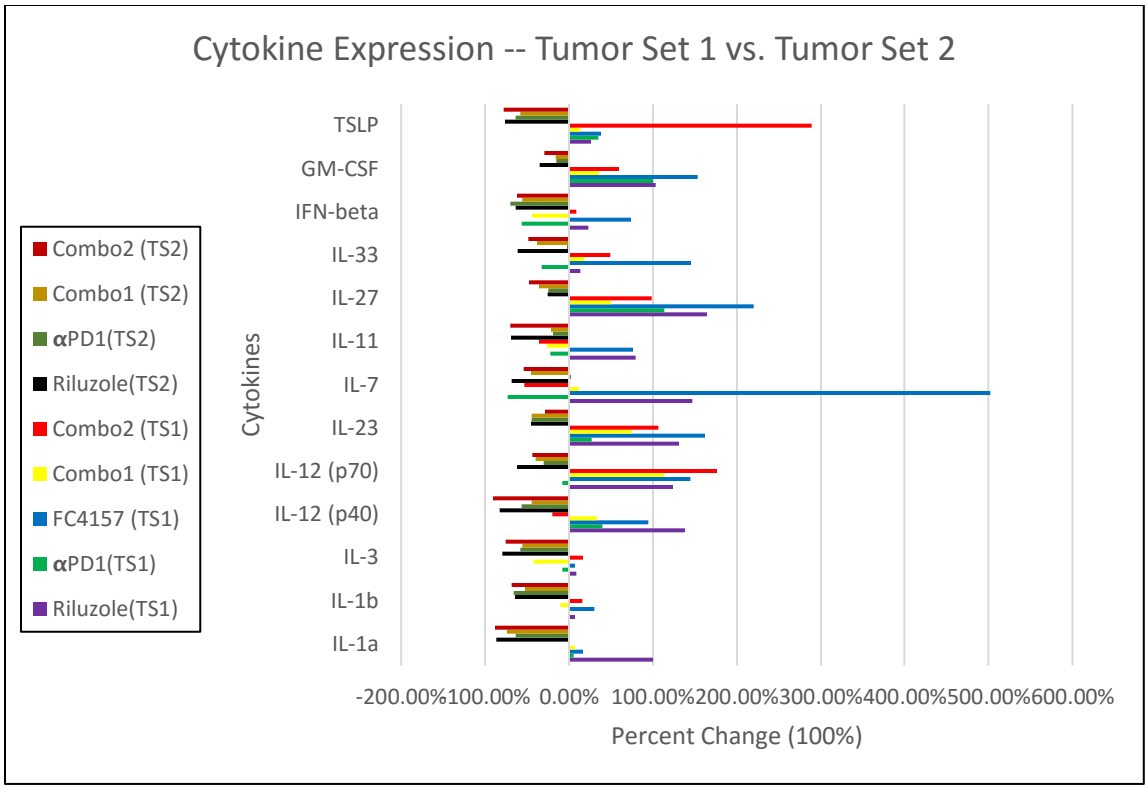

Figure 10. Cytokine expression patterns vary between tumor sets one and two.

Cytokine levels, measured by ELISA array of tumors collected during necropsy, show different expression patterns between tumor set 1 (TS1) and tumor set 2 (TS2). Tumor set 1 data is shown in brighter colored bars, while data from tumor set 2 is shown in darker colored bars.

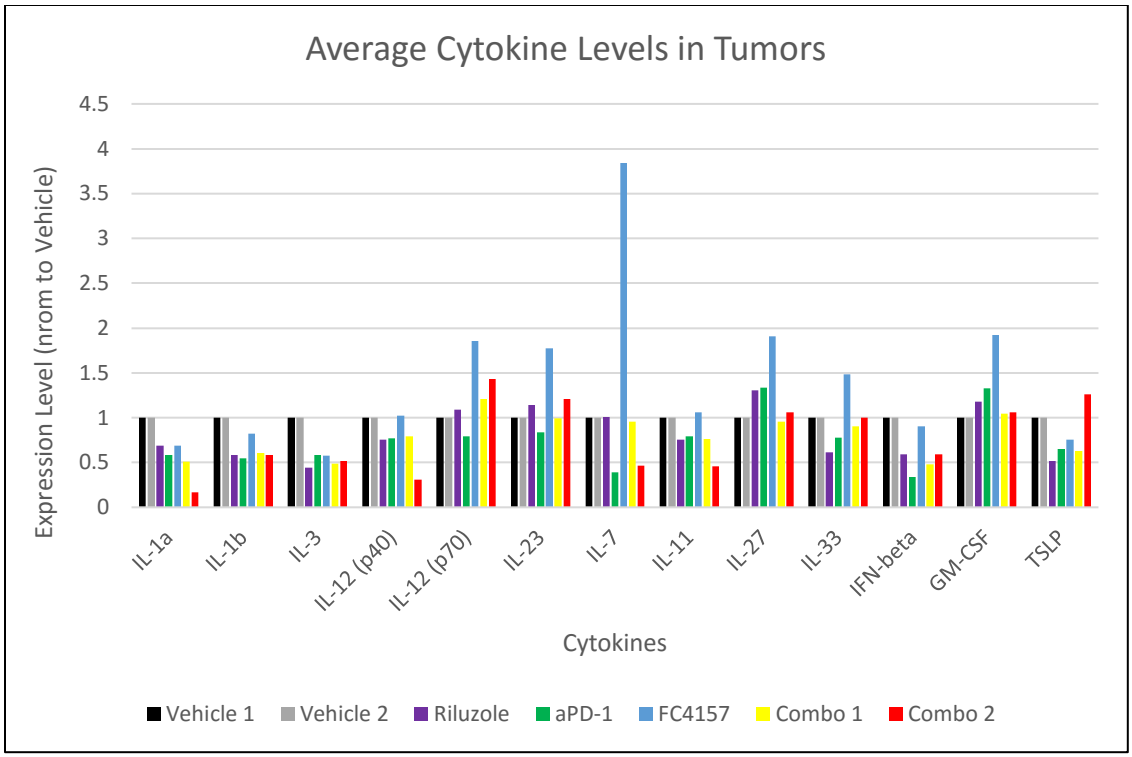

Figure 11. Cytokine expression based on averages of each treatment group from tumor sets one and two.

Cytokine expression levels from ELISA arrays were averaged for each treatment group and normalized to the levels seen in respective vehicle treatments. As tumor set two lacked tissue from an animal in the FC4157 treatment group, the data for this group is based only on the data generated from tissue in tumor set one.

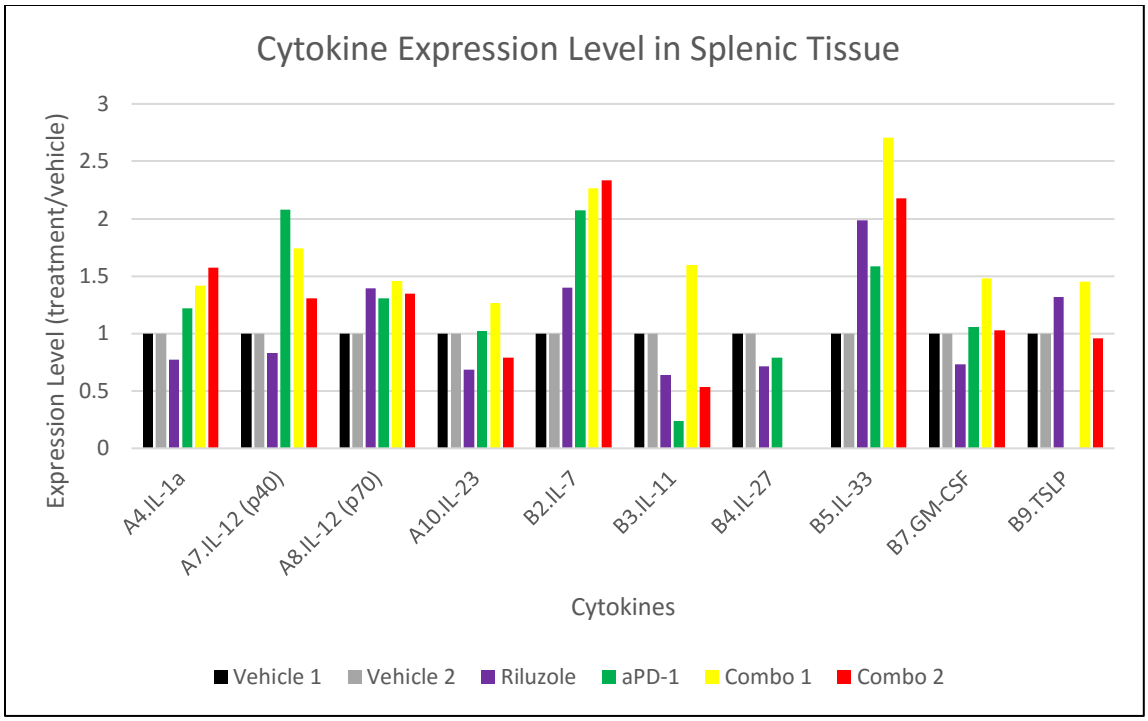

Figure 12. Cytokine expression levels in splenic tissue.
Cytokine expression levels, as determined by ELISA array, were normalized to the respective vehicle groups, for each treatment group. As no splenic tissue was available from the FC4157 treatment group, this group is not represented.

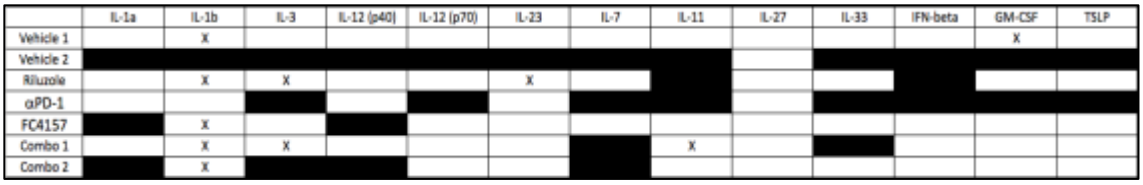

Figure 13. Changes to cytokine expression in serum, as compared to time point zero.

Increases to cytokine expression are shown in black, while decreases are shown in white. **X** in any box indicates data was insufficient to accurately determine increase or decrease. Serum was collected at time point zero, before Mass20 cell injection and before treatment initiation. Serum was also collected at end point, before necropsy. Time point zero data from two sets of serum for each treatment group were averaged, as were end point data. The averaged time points were used to determine changes to cytokines for all treatment groups. Increases are shown in black, while decreases are shown in white.

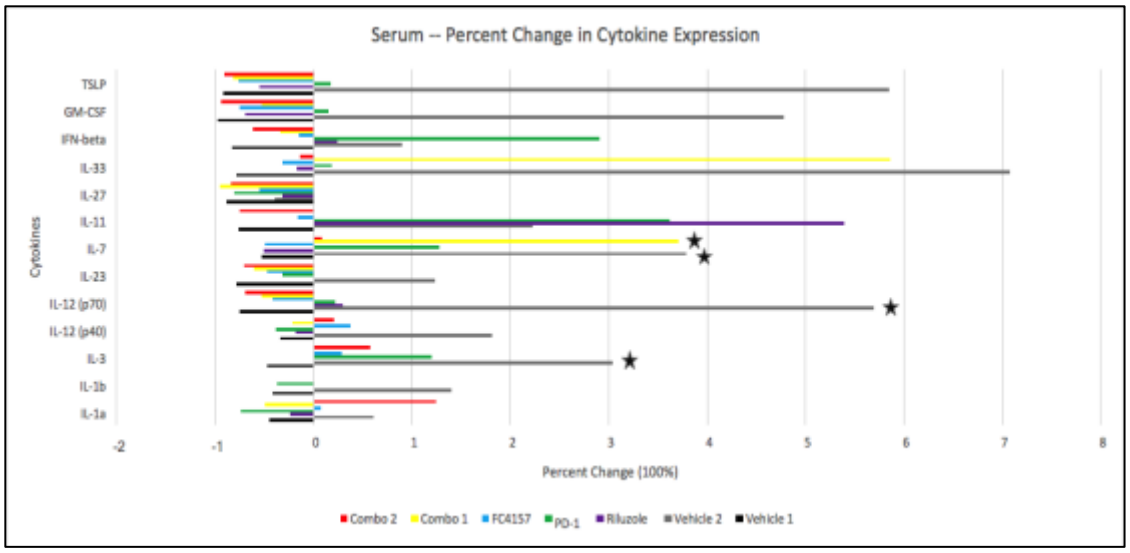

Figure 14. Percent change in cytokine expression between time point 0 and endpoint in serum samples.

Time point 0 and endpoint data for two sets of serum samples were averaged. From the averages, percent change from time point 0 and endpoint was calculated. Bars noted with black stars (Vehicle 2: IL-12 (p70), IL-7, Il-3; Combination 1: IL-7) are 10 fold higher than displayed. These data points were reduced to allow for improved chart readability.

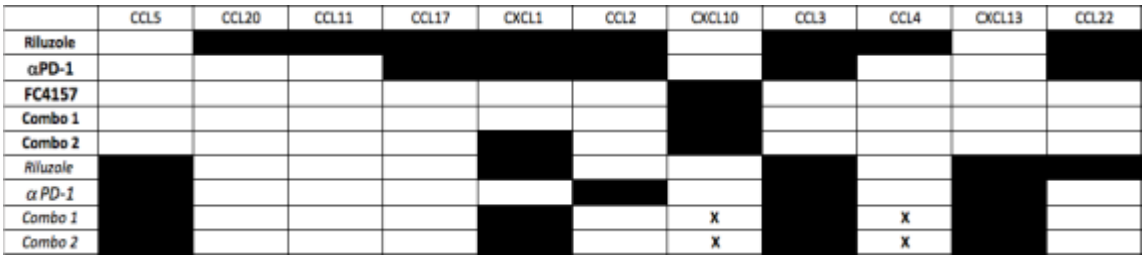

Figure 15. Changes to chemokine expression, as compared to vehicle treatment.

Changes to chemokine expression levels by treatment group, for each chemokine assayed, are shown. Data from tumor sets one and two were averaged. Tumor tissues are indicated by bold text, while splenic tissues are indicated by italic text. Increases are shown in black, while decreases are shown in white. **X** in any box indicates data was insufficient to accurately determine increase or decrease.

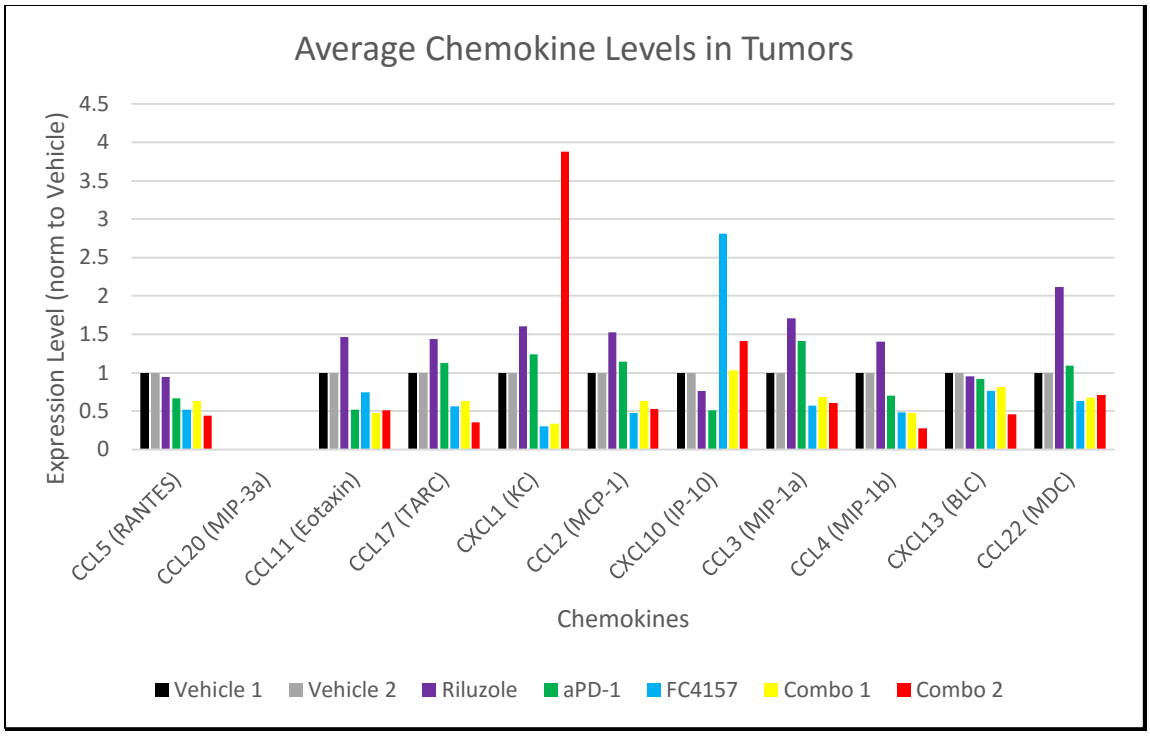

Figure 16. Chemokine expression based on averages of each treatment group from tumor sets one and two.

Chemokine expression levels from ELISA arrays were averaged for each treatment group and normalized to the levels seen in respective vehicle treatments. As tumor set two lacked tissue from the FC4157 treatment group, the data for this group is based only on the data generated from tissue in tumor set one.

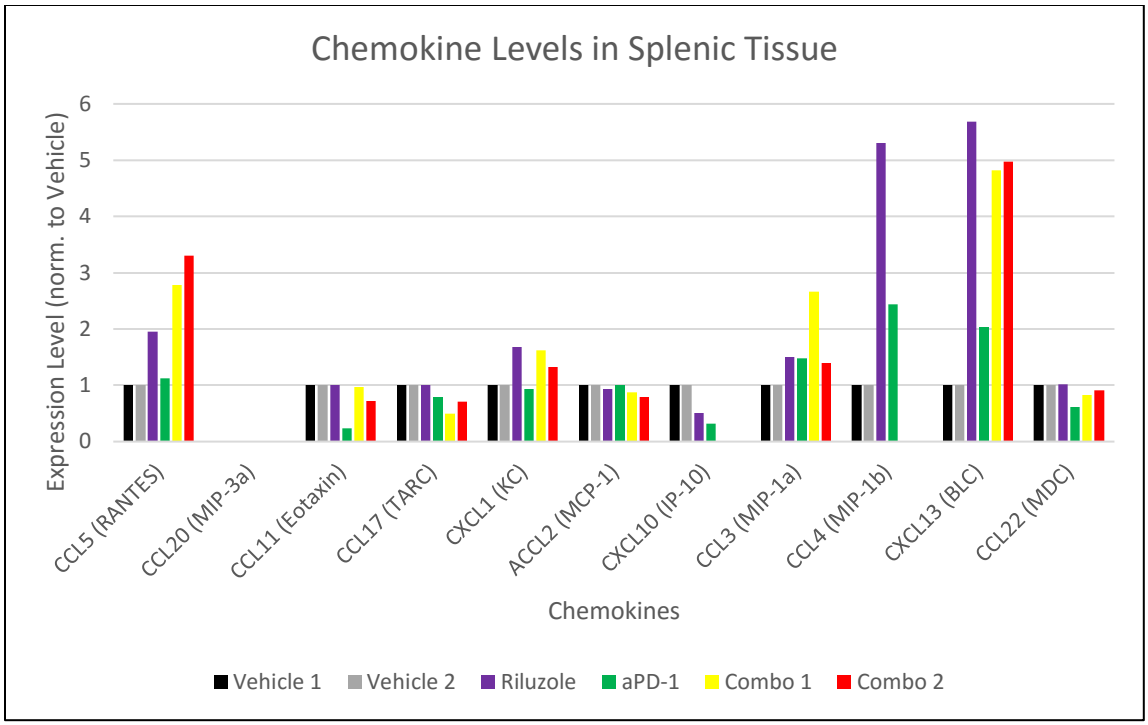

Figure 17. Chemokine expression based on ELISA array analysis of splenic tissue.

Chemokine expression levels were normalized to the levels observed in respective vehicle treated groups. As no splenic tissue was available from the FC4157 treatment group, this group is not represented in this analysis.

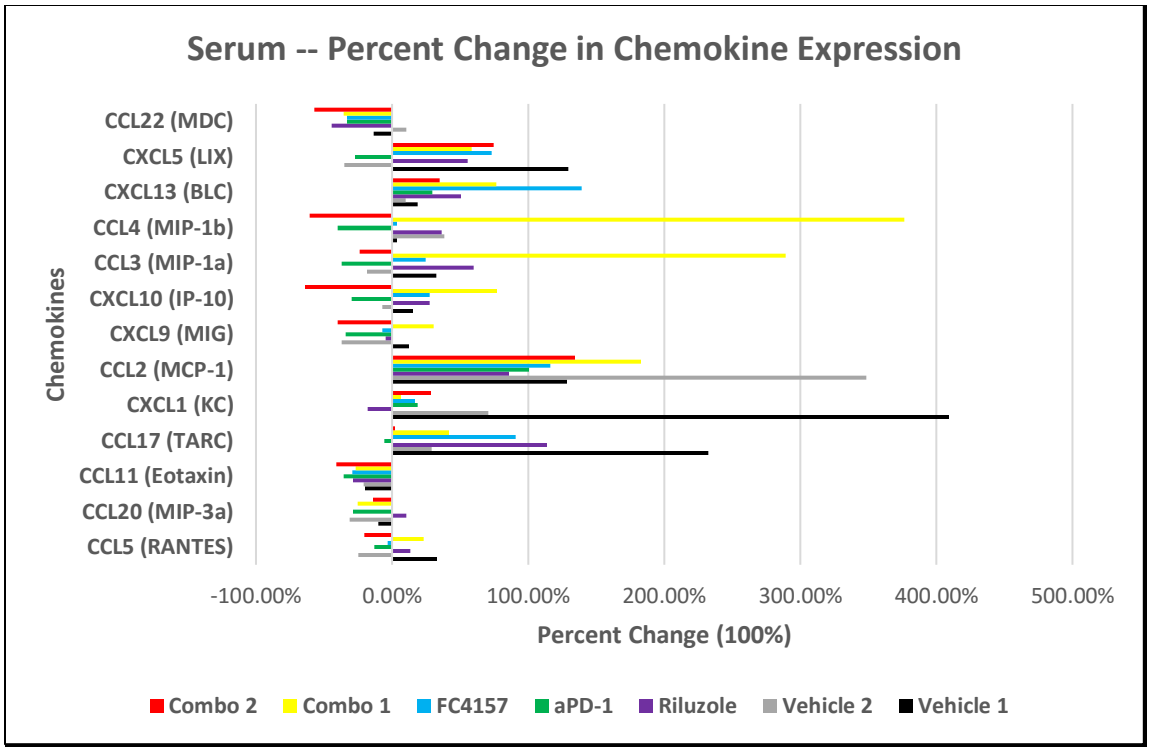

Figure 18. Percent change in average chemokine expression between time point 0 and endpoint in serum samples.
Serum from two animals from each treatment group was collected at time point 0, before Mass20 injection and treatment initiation, and endpoint, just before sacrifice. Chemokine expression levels of each time point, for each animal were averaged and the percent change between the time points is shown above.